Three-Dimensional Transient Electromagnetic Modeling Using Rational Krylov Methods

Börner, Ralph-Uwe and Ernst, Oliver G. and Güttel, Stefan

2014

MIMS EPrint: **2014.36**

Manchester Institute for Mathematical Sciences
School of Mathematics

The University of Manchester

Reports available from: http://eprints.maths.manchester.ac.uk/
And by contacting: The MIMS Secretary
School of Mathematics
The University of Manchester
Manchester, M13 9PL, UK

ISSN 1749-9097

Three-Dimensional Transient Electromagnetic Modeling Using Rational Krylov Methods

Ralph-Uwe Börner, Oliver G. Ernst, and Stefan Güttel

Thursday 24th July, 2014

SUMMARY
A computational method is given for solving the forward modeling problem for transient electromagnetic exploration. Its key features are discretization of the quasi-static Maxwell's equations in space using the first-kind family of curl-conforming Nédélec elements combined with time integration using rational Krylov subspace methods. We show how rational Krylov subspace methods may be used to solve the same problem in the frequency domain followed by a synthesis of the transient solution using the fast Hankel transform, arguing that the pure time-domain is more efficient. We also propose a simple method for selecting the pole parameters of the rational Krylov subspace method which leads to convergence within an a priori determined number of iterations independent of mesh size and conductivity structure. These poles are repeated in a cyclic fashion, which, in combination with direct solvers for the discrete problem, results in significantly faster solution times than previously proposed schemes.

Key words: EM modeling, transient electromagnetics, Krylov subspace methods

1 INTRODUCTION

The rapid numerical inversion and simulation of 3-D electromagnetic (EM) measurements to obtain maps of electromagnetic conductivity of subsurface regions of interest remains one of the major computational challenges of geoelectromagnetic prospecting. The forward simulation or modeling step, in which the response of a given conductivity distribution is computed, is a key element in the inversion process since it must be carried out multiple times for each inversion. The availability of fast forward modeling codes is therefore of crucial importance.

A broad distinction in EM forward modeling schemes is between *time-domain* and *frequency-domain* methods. In the first, the time evolution of electromagnetic fields is propagated forward in time, whereas in the latter the Fourier components of these fields are computed for a suitable collection of frequencies, which are then transformed numerically to the time domain. Both approaches are mathematically equivalent and, as we demonstrate below, can be approximated to desired accuracy using rational Krylov subspace approximations; however, as will become clear, simpler and more accurate numerical methods for TEM forward modeling result when performing all calculations in the time domain.

The finite-difference time-domain (FDTD) scheme introduced by Yee (1966) based on staggered tensor product grids in space has been widely used to model responses of 2-D and 3-D conductivity structures by time-stepping (Taflove 1995). The Yee discretization combined with explicit and implicit time-stepping also forms the basis of transient electromagnetic modeling in the geophysics literature. Among these are Oristaglio and Hohmann (1984), where the 2-D problem of transient electromagnetics is solved with an explicit time-integration scheme proposed by DuFort and Frankel (1953) combined with an upward continuation boundary condition at the air-Earth interface. This approach was extended to model 3-D inhomogeneities in Wang and Hohmann (1993). Commer and G. Newman (2004) present a finite difference scheme for the simulation of transient electromagnetic fields generated by galvanic sources. They were able to compute the initial conditions by solving a stationary 3-D Poisson problem, as it appears, e.g., in the numerical solution of the 3-D DC resistivity problem. Moreover, their algorithm was designed to run on parallel computer architectures.

The stability constraints of explicit time-stepping schemes for the parabolic quasi-static Maxwell equations require excessively small time steps for fine spatial resolution. Although each time step consists of essentially a matrix-vector product, small time steps can lead to high computational demands. As demonstrated in Oristaglio and Hohmann (1984), the DuFort-Frankel method allows the time step to increase with the square root of simulation time as the integration progresses.

Unlike explicit schemes, implicit methods solve a linear systems of equations to obtain the solution for each desired time step. M. M. Goldman and Stoyer (1983) have simulated transients for 2-D structures with axial symmetry by implicit time-stepping. Haber et al. (2002) simulated 3-D transients employing a backward Euler scheme, a variant of the implicit time-stepping method. At each time step, they solved the system of linear equations arising from a finite volume discretization. The system was solved with a preconditioned biconjugate gradient method.

Transient electromagnetic fields may also be obtained by inverse Fourier transformation of sufficiently many frequency-domain solutions. G. A. Newman et al. (1986) implemented an integral equation formulation in the frequency domain, and transformed the solutions back to the time domain using a fast Han-

kel transform. A similar approach was proposed by Mulder et al. (2008), who compute a small number of frequency-domain solutions and transform a spline-interpolated set of solutions to the time domain. The discrete times for which a transient can be calculated depend on the sampling interval as well as the bandwidth of the discrete solutions given in the frequency domain. Generally, for a transient spanning from very early to late times, e.g., from 10^{-6} to 10^{-3} seconds, many—typically around 100—frequency-domain solves are necessary, which requires an unreasonably high numerical effort.

Improvements over explicit or implicit time-stepping can be achieved using Krylov subspace methods. Like time-stepping, Krylov subspace methods for solving the quasi-static Maxwell's equations require a matrix vector product or linear system solve at each iteration. However, the approximations at the desired time values are obtained by choosing a near-best approximation from a global subspace whose dimension increases with each Krylov iteration. For the frequency-domain approach the solution at the desired frequencies required for Fourier synthesis are approximated in a similar fashion. V. L. Druskin and Knizhnerman (1988) used a spectral Lanczos decomposition method to obtain an arbitrary number of frequency-domain solution at a substantially lower numerical cost. Moreover, they pioneered the use of Krylov subspace methods to evaluate transients directly in the time domain (V. L. Druskin and Knizhnerman 1994; V. L. Druskin, Knizhnerman, and Lee 1999) and subsequently extended their research towards rational Krylov methods (Knizhnerman et al. 2009; V. L. Druskin, Knizhnerman, and Zaslavsky 2009; V. Druskin, Lieberman, et al. 2010; V. Druskin and Zaslavsky 2011; V. L. Druskin and Simoncini 2011; Zaslavsky et al. 2011; V. Druskin, Remis, et al. 2014). Börner et al. (2008) combined a shift-and-invert Krylov subspace projection method to evaluate the matrix resolvent function in the frequency domain, and the Fourier method to transform the obtained solutions back to time domain using a fast Hankel transform.

In this paper, which is an extension of Börner et al. (2008) to the time domain as well as higher order rational Krylov subspace approximations, we demonstrate how optimal values of the parameters which determine a rational Krylov method known as *poles* can be obtained *a priori* using a surrogate optimization technique. The resulting poles are problem and mesh independent, and thus do not change with discretization features such as the mesh size or spectral interval of the system matrices. This property can be exploited to model conductivity structures with large coefficient jumps, which appear naturally when topography has to be included in the geophysical model. Moreover, our approach produces a cyclic pole sequence consisting of a small number of distinct poles selected to guarantee an a priori determined level of accuracy in the transient within a known number of iterations. When combined with direct methods for the solution of the discrete linear systems, this leads to considerable computational savings, since the number of matrix factorizations equals the number of distinct poles employed (here between one and four). In particular, the computational work for the factorizations can be amortized over all rational Krylov iterations. An additional benefit of using cyclically repeated poles is that the linear systems associated with each pole can be solved concurrently in a parallel computing environment. In this case a larger number of cyclically repeated poles can be chosen to match the number of available processing units.

The remainder of this paper is organized as follows: We first recall in Section 2 the governing partial differential equations (PDEs) of geoelectromagnetic induction in the time and frequency domains and relate these via the Fourier transform. This is followed by a description of the spatial discretization using Nédélec finite elements on a tetrahedral mesh, specifying the discrete solutions in the time and frequency domains. We reformulate the problem in terms of matrix functions and demonstrate how a solution can be obtained by a rational Arnoldi approximation. In Section 3 we derive the rational Arnoldi method for the evaluation of the action of a function of a matrix on a given vector and show how this can be applied to solve the discrete problem in the time and frequency domains. We show how optimal poles can be chosen for the rational Krylov method for which the approximation converges uniformly with respect to both spatial mesh size and conductivity structure. We conclude in Section 4 with two numerical examples. As a first problem, we deal with a simple model of a layered half-space to demonstrate that our approach yields accurate results. We compare the results obtained by our method to results obtained by inverse Fourier transform of large-scale frequency-domain solutions. The choice of this simple model ensures that our results can be compared to an analytical solution. As a second numerical example, we show the performance of our method for a homogeneous half-space with topography.

2 MATHEMATICAL MODEL AND DISCRETIZATION

2.1 Governing Equations

We begin by recalling the governing equations of electromagnetic induction. Neglecting displacement currents and eliminating the magnetic field, the time-dependent Maxwell's equations for the electric field intensity $\boldsymbol{e} = \boldsymbol{e}(\boldsymbol{x}, t)$ read

$$\sigma \partial_t \boldsymbol{e} + \nabla \times (\mu^{-1} \nabla \times \boldsymbol{e}) = -\partial_t \boldsymbol{j}^e, \qquad t \in \mathbb{R}. \tag{1}$$

The spatial coordinate $\boldsymbol{x}$ is assumed to vary in a computational domain $\Omega \subset \mathbb{R}^3$ containing the air-Earth interface. The magnetic permeability $\mu = \mu_0 = 4\pi \cdot 10^{-7}$ Vs/Am is that of free space and the electric conductivity $\sigma = \sigma(\boldsymbol{x})$ is a given function defined on Ω. Along the boundary $\partial\Omega$ of Ω we impose the perfect conductor boundary condition

$$\boldsymbol{n} \times \boldsymbol{e} = \boldsymbol{0}, \tag{2}$$

and we make the implicit assumption that the boundary has been placed at sufficient distance from sources that the effects of the boundary conditions are negligible compared to discretization errors.

2.2 Source Terms

We consider a source density $\boldsymbol{j}^e$ resulting from a stationary transmitter with a driving current that is shut off at time $t = 0$, giving

$$\boldsymbol{j}^e(\boldsymbol{x}, t) = \boldsymbol{q}(\boldsymbol{x}) H(-t), \tag{3}$$

in which H denotes the Heaviside unit step function and the vector field $\boldsymbol{q}$ denotes the spatial current pattern. Specifically, we consider a transmitter consisting of a small horizontal square wire-loop carrying a stationary current, thus generating a good approximation of a vertical magnetic dipole. In particular, we note that the resulting current density is divergence-free, i.e.,

$$\nabla \cdot \boldsymbol{q} = 0. \tag{4}$$

2.3 Time-Domain Formulation

Denoting by $\delta(t) = \partial_t H(t)$ the Dirac delta distribution concentrated at the origin $t = 0$, the combination of (1), (2) and (3) results in the boundary value problem

$$\sigma\partial_t \boldsymbol{e} + \nabla\times(\mu^{-1}\nabla\times\boldsymbol{e}) = \boldsymbol{q}(\boldsymbol{x})\delta(t) \quad \text{on } \Omega\times\mathbb{R}, \tag{5a}$$

$$\boldsymbol{n}\times\boldsymbol{e} = \boldsymbol{0} \quad \text{along } \partial\Omega \tag{5b}$$

for the electric field intensity $\boldsymbol{e}$ as a function of time and space on the entire time axis. For time-domain simulations it is more convenient to formulate (5) as the initial-boundary value problem

$$\sigma\partial_t \boldsymbol{e} + \nabla\times(\mu^{-1}\nabla\times\boldsymbol{e}) = \boldsymbol{0} \quad \text{on } \Omega\times(0,\infty), \tag{6a}$$

$$\boldsymbol{e}|_{t=0} = \boldsymbol{q} \quad \text{on } \Omega, \tag{6b}$$

$$\boldsymbol{n}\times\boldsymbol{e} = \boldsymbol{0} \quad \text{on } \partial\Omega\times(0,\infty). \tag{6c}$$

2.4 Frequency-Domain Formulation

To formulate the same problem in the frequency domain, we apply the Fourier transform in time, denoted by the operator $\mathscr{F}$, to both sides of (1), and introduce the transformed electric field

$$\boldsymbol{E}(\boldsymbol{x},\omega) := (\mathscr{F}\boldsymbol{e})(\omega) = \int_{-\infty}^{\infty} \boldsymbol{e}(\boldsymbol{x},t)\,\mathrm{e}^{-i\omega t}\,\mathrm{d}t, \qquad \omega\in\mathbb{R},$$

where the *angular frequency* ω has units rad/s. Observing the the correspondence $(\mathscr{F}H)(\omega) = \pi\delta(\omega) + \frac{1}{i\omega}$, where δ denotes the Dirac delta distribution concentrated at zero, as well as the scaling and derivative laws for the Fourier transform, we obtain the frequency-domain equation

$$\nabla\times(\mu^{-1}\nabla\times\boldsymbol{E}) + i\omega\sigma\boldsymbol{E} = -i\omega\boldsymbol{q}\left(\pi\delta(\omega) - \frac{1}{i\omega}\right), \qquad \omega\in\mathbb{R}. \tag{7}$$

To simplify the problem, we introduce the impulse response electric field $\boldsymbol{e}_i = \boldsymbol{e}_i(\boldsymbol{x},t)$ as the solution of (1) with impulsive source current $\boldsymbol{j}_i^e(\boldsymbol{x},t) = \boldsymbol{q}(\boldsymbol{x})\delta(t)$. In view of the relation $(\mathscr{F}\delta)(\omega)\equiv 1$, its Fourier transform $\boldsymbol{E}_i = \boldsymbol{E}_i(\boldsymbol{x},\omega)$ satisfies

$$\nabla\times(\mu^{-1}\nabla\times\boldsymbol{E}_i) + i\omega\sigma\boldsymbol{E}_i = -i\omega\boldsymbol{q}. \tag{8}$$

We note that the fields $\boldsymbol{E}$ and $\boldsymbol{E}_i$ in equations (7) and(8) satisfy the same homogeneous boundary condition (2) and the same PDE with right-hand sides which are both scalar multiples of $\boldsymbol{q}$, implying

$$\boldsymbol{E}(\omega) = \left(\pi\delta(\omega) - \frac{1}{i\omega}\right)\boldsymbol{E}_i(\omega). \tag{9}$$

Transforming back to the time domain results in the transient solution

$$\begin{aligned}\boldsymbol{e}(\boldsymbol{x},t) &= \frac{1}{2\pi}\int_{-\infty}^{\infty}\boldsymbol{E}(\boldsymbol{x},\omega)\,e^{i\omega t}\,\mathrm{d}\omega\\ &= \frac{1}{2\pi}\int_{-\infty}^{\infty}\left(\pi\delta(\omega)-\frac{1}{i\omega}\right)\boldsymbol{E}_i(\omega)\,e^{i\omega t}\,\mathrm{d}\omega\\ &= \frac{1}{2}\boldsymbol{E}_i(0) - \frac{1}{2\pi}\int_{-\infty}^{\infty}\frac{\boldsymbol{E}_i(\omega)}{i\omega}\,e^{i\omega t}\,\mathrm{d}\omega \qquad t\in\mathbb{R}\end{aligned} \tag{10}$$

where the DC component $\boldsymbol{E}_i(0)$ vanishes since the source field $\boldsymbol{q}$ is divergence-free.

2.5 Finite Element Discretization

Our numerical approximation for both the time- and frequency-domain formulations is based on a finite element discretization in space using first-kind Nédélec spaces on unstructured tetrahedral meshes. A theoretical background on Nédélec elements can be found in Monk (2003); their implementation is described in Gopalakrishnan et al. (2005) and Kirby (2014).

2.5.1 Variational Formulation

The standard variational formulation for Maxwell's equations seeks the electric field in the Sobolev space

$$\boldsymbol{H}(\mathrm{curl};\Omega) = \{\boldsymbol{u}\in L^2(\Omega)^3 : \nabla\times\boldsymbol{u}\in L^2(\Omega)^3\}.$$

Since we impose the homogeneous boundary condition (2) along the entire boundary $\partial\Omega$, we restrict the fields further to the subspace

$$\mathscr{V} := \{\boldsymbol{u}\in\boldsymbol{H}(\mathrm{curl};\Omega) : \boldsymbol{n}\times\boldsymbol{u} = \boldsymbol{0} \text{ along } \partial\Omega\}.$$

Multiplying (6) by an arbitrary stationary vector field $\boldsymbol{\phi}\in\mathscr{V}$ and integrating by parts yields the variational problem of seeking $\boldsymbol{e} = \boldsymbol{e}(\boldsymbol{x},t)\in C([0,\infty);\mathscr{V})$ such that

$$(\sigma\partial_t\boldsymbol{e},\boldsymbol{\phi}) + (\mu^{-1}\nabla\times\boldsymbol{e},\nabla\times\boldsymbol{\phi}) = \boldsymbol{0}, \qquad t\in(0,\infty), \tag{11a}$$

$$(\boldsymbol{e}|_{t=0},\boldsymbol{\phi}) = (\boldsymbol{q},\boldsymbol{\phi}), \tag{11b}$$

for all $\boldsymbol{\phi}\in\mathscr{V}$, where $(\cdot,\cdot)$ denotes the inner product on $L^2(\Omega)^3$.

2.5.2 Discretization in Space

We employ a Galerkin discretization in space obtained by restricting the trial and test functions $\boldsymbol{e}$ and $\boldsymbol{\phi}$ in the weak form (11) to a finite-dimensional subspace $\mathscr{V}^h\subset\mathscr{V}$ consisting of first-kind Nédélec finite elements on a tetrahedral mesh $\mathscr{T}_h$. Nédélec elements are a natural approximation of electromagnetic vector fields in that they are curl-conforming, i.e., they mimic the tangential continuity properties of the fields under approximation, permitting jumps in the normal field components whenever the conductivity is discontinuous across an interfaces. On each tetrahedron $K\in\mathscr{T}_h$ the functions in $\mathscr{V}^h$ consist of vector polynomials $\boldsymbol{v}\in\mathscr{P}_{k-1}^3\oplus\mathscr{S}_k$,, where $\mathscr{P}_k$ denotes the space of polynomials in three variables of complete degree $k\in\mathbb{N}_0$ and

$$\mathscr{S}_k = \{\boldsymbol{v}\in\widetilde{\mathscr{P}}_k^3 : \boldsymbol{v}\cdot\boldsymbol{x} = \boldsymbol{0}\}$$

with $\widetilde{\mathscr{P}}_k$ denoting the space of homogeneous polynomials of (exact) degree k. In our numerical experiments we have used Nédélec elements of order $k=1$ and $k=2$, sometimes also known as *linear* and *quadratic* Nédélec elements. The discrete approximation of the solution of the variational formulation (11) is then obtained by restricting it to the subspace $\mathscr{V}^h$, i.e., by determining $\boldsymbol{e}^h\subset\mathscr{V}^h$ such that, for all test functions $\boldsymbol{\phi}\in\mathscr{V}^h$, there holds

$$(\sigma\partial_t\boldsymbol{e}^h,\boldsymbol{\phi}) + (\mu^{-1}\nabla\times\boldsymbol{e}^h,\nabla\times\boldsymbol{\phi}) = \boldsymbol{0}, \qquad t\in(0,\infty), \tag{12a}$$

$$(\boldsymbol{e}^h|_{t=0},\boldsymbol{\phi}) = (\boldsymbol{q},\boldsymbol{\phi}). \tag{12b}$$

Expanding the discrete solution $\boldsymbol{e}^h\in\mathscr{V}^h$ in a basis $\{\boldsymbol{\phi}_1,\ldots,\boldsymbol{\phi}_N\}$ of $\mathscr{V}^h$, (12) becomes the ODE initial-value problem

$$\mathbf{M}\partial_t\mathbf{u}(t) + \mathbf{C}\mathbf{u}(t) = \mathbf{0}, \quad t\in(0,\infty) \qquad \mathbf{M}\mathbf{u}(0) = \mathbf{q}, \tag{13}$$

for the vector $\mathbf{u}(t)$ containing the N coefficients of the finite element approximation $\boldsymbol{e}^h(t)$ with respect to the Nédélec basis at time

$t \geq 0$. Here the mass and curl-curl matrices $\mathbf{M}$ and $\mathbf{C}$ as well as the vector $\mathbf{q}$ of initial values are given in terms of the Nédélec basis by

$$[\mathbf{M}]_{i,j} = (\sigma\boldsymbol{\phi}_j, \boldsymbol{\phi}_i), \quad [\mathbf{C}]_{i,j} = (\mu^{-1}\nabla\times\boldsymbol{\phi}_j, \nabla\times\boldsymbol{\phi}_i), \quad i,j = 1,\ldots,N,$$
$$[\mathbf{q}]_i = (\boldsymbol{q}, \boldsymbol{\phi}_i), \qquad i = 1,\ldots,N.$$

For the frequency-domain formulation we may employ the same spatial discretization, in terms of which (8) becomes the linear system of equations

$$(\mathbf{C} + i\omega\mathbf{M})\mathbf{u}(\omega) = -i\omega\mathbf{q} \tag{14}$$

for the coefficient vector $\mathbf{u}(\omega)$ of the impulse-response solution at frequency ω with respect to the Nédélec basis.

2.5.3 Representation as Matrix Functions

The explicit solution of the semi-discretized time-domain problem (13) is given in terms of the matrix exponential function

$$\mathbf{u}(t) = \exp(-t\mathbf{M}^{-1}\mathbf{C})\mathbf{M}^{-1}\mathbf{q} = f^t(\mathbf{A})\mathbf{b}, \tag{15}$$

with

$$f^t(z) = \exp(-tz), \quad \mathbf{A} = \mathbf{M}^{-1}\mathbf{C}, \quad \mathbf{b} = \mathbf{M}^{-1}\mathbf{q}.$$

Similarly, the finite element discretization (14) of the frequency-domain problem (8) has the solution

$$\mathbf{u}(\omega) = -i\omega(\mathbf{C} + i\omega\mathbf{M})^{-1}\mathbf{q} = -i\omega(\mathbf{A} + i\omega\mathbf{I})^{-1}\mathbf{b} = g^\omega(\mathbf{A})\mathbf{b}, \tag{16}$$

with

$$g^\omega(z) = \frac{i\omega}{z + i\omega}.$$

Applying the inverse Fourier transform (10) back to the time domain to the discrete frequency-domain solution vector $\mathbf{u}(\omega)$ yields

$$(\mathscr{F}^{-1}\mathbf{u})(t) = \frac{1}{2\pi}\int_{-\infty}^{\infty}(\mathbf{A} + i\omega\mathbf{I})^{-1}\mathbf{b}e^{i\omega t}\,\mathrm{d}\omega. \tag{17}$$

To show that the transformed discrete frequency-domain solution agrees with that of the time domain, we express the latter using contour integration. Recall that, as an entire function, the function f^t in (15) may be represented as the Cauchy integral

$$f^t(z) = \frac{1}{2\pi i}\int_\Gamma \frac{f^t(\zeta)}{\zeta - z}\,\mathrm{d}\zeta, \tag{18}$$

where Γ is a contour surrounding the point z in the complex plane. The same contour integral may be used to evaluate $f^t(\mathbf{A})$ provided the contour Γ contains all eigenvalues of $\mathbf{A}$ in its interior. Since

$$\mathbf{M}^{1/2}\mathbf{A}\mathbf{M}^{-1/2} = \mathbf{M}^{-1/2}\mathbf{C}\mathbf{M}^{-1/2},$$

we see that $\mathbf{A}$ is similar to the matrix on the right-hand side, which is symmetric and, since $\mathbf{M}$ is symmetric positive definite and $\mathbf{C}$ symmetric positive semidefinite, is also symmetric positive semidefinite. The eigenvalues of $\mathbf{A}$ therefore lie on the nonnegative real axis. The zero eigenvalues of $\mathbf{C}$ are associated with discrete gradient fields. These are not present in the given solution due to the fact that the field $\boldsymbol{q}$ is divergence-free. We may therefore ignore the zero eigenvalue and use the imaginary axis as the integration contour in (18). Parametrizing the imaginary axis by $-i\omega$, $\omega \in (-\infty, \infty)$, we obtain

$$\mathbf{u}(t) = f^t(\mathbf{A})\mathbf{b} = \frac{1}{2\pi i}\int_\Gamma (\zeta\mathbf{I} - \mathbf{A})^{-1} f^t(\zeta)\,\mathrm{d}\zeta\;\mathbf{b} = \frac{1}{2\pi}\int_{-\infty}^{\infty}(\mathbf{A} + i\omega\mathbf{I})^{-1}e^{i\omega t}\mathbf{b}\,\mathrm{d}\omega,$$

which coincides with (17).

3 RATIONAL ARNOLDI APPROXIMATION

We have seen in the previous section that the space-discretized solution (15) at time t as well as the frequency-domain solution (16) at frequency ω can be expressed as the result of either the matrix exponential or resolvent function applied to a given vector. When the matrix in question is large and sparse, as arises in the discretization of partial differential operators such as Maxwell's equations, Krylov subspace approximations can be applied to obtain efficient solution methods. In this section we briefly recall a very general Krylov subspace algorithm known as the rational Arnoldi method for approximating the action $f(\mathbf{A})\mathbf{b}$, $\mathbf{A} = \mathbf{M}^{-1}\mathbf{C}$, of a generic matrix function f using an orthogonalization procedure in the $\mathbf{M}$-inner product defined as $\langle \mathbf{x}, \mathbf{y}\rangle_\mathbf{M} := \mathbf{y}^H\mathbf{M}\mathbf{x}$ with induced norm $\|\mathbf{x}\|_\mathbf{M} := \sqrt{\langle \mathbf{x}, \mathbf{x}\rangle_\mathbf{M}}$. Here $\mathbf{y}^H$ denotes the complex conjugate transpose of $\mathbf{y}$. In the application to the discretized Maxwell operator the symmetric positive definite matrix $\mathbf{M}$ defining the inner product will be the finite element mass matrix, which is the continuous $L^2(\Omega)$ inner product restricted to the finite element space. Starting with the vector $\mathbf{v}_1 = \mathbf{b}/\|\mathbf{b}\|_\mathbf{M}$, we construct the basis vector $\mathbf{v}_{j+1}$ $\mathbf{M}$-orthogonal to $\mathbf{v}_1, \mathbf{v}_2, \ldots, \mathbf{v}_j$ using the recursion

$$\mathbf{v}_{j+1}h_{j+1,j} = (\mathbf{I} - \mathbf{A}/\xi_j)^{-1}\mathbf{A}\mathbf{v}_j - \sum_{i=1}^{j}\mathbf{v}_i h_{i,j}.$$

Collecting these basis vectors in a matrix $\mathbf{V}_{m+1} = [\mathbf{v}_1, \mathbf{v}_2, \ldots, \mathbf{v}_{m+1}] \in \mathbb{C}^{N\times(m+1)}$ and the orthogonalization coefficients in the upper Hessenberg matrix $\underline{\mathbf{H}_m} = [h_{i,j}] \in \mathbb{C}^{(m+1)\times m}$, it is easily verified that these quantities satisfy a *rational Arnoldi decomposition* (see Ruhe (1994a) and Ruhe 1994b)

$$\mathbf{A}\mathbf{V}_{m+1}(\underline{\mathbf{I}_m} + \underline{\mathbf{H}_m}\mathbf{X}_m) = \mathbf{V}_{m+1}\underline{\mathbf{H}_m},$$

where $\mathbf{X}_m = \mathrm{diag}(\xi_1^{-1}, \xi_2^{-1}, \ldots, \xi_m^{-1}) \in \mathbb{C}^{m\times m}$ and $\underline{\mathbf{I}_m} \in \mathbb{C}^{(m+1)\times m}$ is the identity matrix with an appended bottom row of zeros. Note that $\mathbf{V}_{m+1}^H\mathbf{M}\mathbf{V}_{m+1} = \mathbf{I}_{m+1}$. Also note that the vector $\mathbf{v}_{m+1}$ depends on the pole ξ_m but this is not so for the remaining Krylov basis vectors $\mathbf{v}_1, \mathbf{v}_2, \ldots, \mathbf{v}_m$; hence we can set $\xi_m = \infty$ without altering the span of $\mathbf{V}_m$. In this case we obtain a *reduced rational Arnoldi decomposition*

$$\mathbf{A}\mathbf{V}_m\mathbf{K}_m = \mathbf{V}_{m+1}\underline{\mathbf{H}_m}, \qquad \mathbf{K}_m = \mathbf{I}_m + \mathbf{H}_m\mathbf{X}_m, \tag{19}$$

which can also be written in the form

$$\mathbf{A}\mathbf{V}_m = \mathbf{V}_m\mathbf{H}_m\mathbf{K}_m^{-1} + h_{m+1,m}\mathbf{v}_{m+1}\mathbf{e}_m^T\mathbf{K}_m^{-1}. \tag{20}$$

Using this decomposition one may construct the *rational Arnoldi approximation of order* m defined by

$$\mathbf{f}_m := \mathbf{V}_m f(\mathbf{H}_m\mathbf{K}_m^{-1})\mathbf{V}_m^H\mathbf{b} \approx f(\mathbf{A})\mathbf{b}. \tag{21}$$

We will see in the following that this approximation enjoys some remarkable properties. Multiplying the decomposition (20) from the left by $\mathbf{V}_m^H\mathbf{M}$, using the facts that $\mathbf{V}_m^H\mathbf{M}\mathbf{v}_{m+1} = \mathbf{0}$ and $\mathbf{A} = \mathbf{M}^{-1}\mathbf{C}$, we find the simple relation

$$\mathbf{V}_m^H\mathbf{M}\mathbf{A}\mathbf{V}_m = \mathbf{V}_m^H\mathbf{C}\mathbf{V}_m = \mathbf{H}_m\mathbf{K}_m^{-1} := \mathbf{A}_m.$$

In principle, the projected $m \times m$ matrix $\mathbf{A}_m$ can be computed at little cost as $\mathbf{H}_m\mathbf{K}_m^{-1}$ from quantities of the reduced rational Arnoldi decomposition (19), however, if $\mathbf{K}_m$ is ill-conditioned this computation may suffer from numerical instabilities. In particular, $\mathbf{H}_m\mathbf{K}_m^{-1}$ may no longer be numerically Hermitian even though $\mathbf{C}$ is. In such cases it is advisable to compute $\mathbf{A}_m$ via explicit projection $\mathbf{V}_m^H\mathbf{C}\mathbf{V}_m$.

We next recall a theorem which characterizes the rational Arnoldi approximation as the action of a rational function r_m

which interpolates the function f. Several variants of this result have appeared in the literature, both for polynomial (Ericsson 1990; Saad 1992) and rational Krylov spaces (Beckermann and Reichel 2009 or Güttel 2010, Theorem 5.8). Here in the following, $\mathscr{P}_{m-1}$ denotes the linear space of all polynomials of degree at most $m-1$, and $\mathscr{P}_{m-1}/q_{m-1}$ is the linear space of rational functions of type $(m-1, m-1)$ with prescribed denominator q_{m-1}.

Theorem 3.1. The rational Arnoldi approximation $\mathbf{f}_m$ of $f(\mathbf{A})\mathbf{b}$ associated with the reduced rational Arnoldi decomposition (19) satisfies

$$\mathbf{f}_m = \mathbf{V}_m f(\mathbf{H}_m \mathbf{K}_m^{-1}) \mathbf{V}_m^H \mathbf{b} = r_m(\mathbf{A})\mathbf{b},$$

where $r_m \in \mathscr{P}_{m-1}/q_{m-1}$ interpolates f in Hermite's sense (i.e., counting multiplicities) at the eigenvalues $\Lambda(\mathbf{H}_m\mathbf{K}_m^{-1}) = \Lambda(\mathbf{V}_m^H\mathbf{C}\mathbf{V}_m)$, where $q_{m-1}(z) = (1 - z/\xi_1)(1 - z/\xi_2)\cdots(1 - z/\xi_{m-1})$.

It follows from Theorem 3.1 that the rational Arnoldi approximation $\mathbf{f}_m$ is exact if f is itself a rational function in $\mathscr{P}_{m-1}/q_{m-1}$, i.e., a rational function of type $(m-1, m-1)$ with prescribed denominator q_{m-1}. This exactness implies that $\mathbf{f}_m$ satisfies a near-optimality property in the $\mathbf{M}$-norm. Similar results for optimality in the 2-norm have been given in (Ericsson 1990; Saad 1992; Beckermann and Reichel 2009; Güttel 2010).

The following result is the key to error analysis of rational Krylov methods and the optimal selection of the poles $\xi_1, \ldots, \xi_{m-1}$, as it bounds the approximation error in terms of the interpolation error of r_m on an interval of the real line:

Theorem 3.2. The rational Arnoldi approximation $\mathbf{f}_m$ for $f(\mathbf{A})\mathbf{b}$ associated with the reduced rational Arnoldi decomposition (19) satisfies

$$\|f(\mathbf{A})\mathbf{b} - \mathbf{f}_m\|_{\mathbf{M}} \leq 2\|\mathbf{b}\|_{\mathbf{M}} \min_{r_m \in \mathscr{P}_{m-1}/q_{m-1}} \max_{z\in[\alpha,\beta]} |f(z) - r_m(z)|, \tag{22}$$

where $[\alpha, \beta]$ is an interval containing the eigenvalues of $\mathbf{A} = \mathbf{M}^{-1}\mathbf{C}$.

Proof: A straightforward calculation using the triangle inequality for vector norms and the fact that $r_m(\mathbf{A})\mathbf{b} = \mathbf{V}_m r_m(\mathbf{A}_m)\mathbf{V}_m^H\mathbf{b}$ by Theorem 3.1 shows

$$\begin{aligned} & \|f(\mathbf{A})\mathbf{b} - \mathbf{f}_m\|_{\mathbf{M}} \\ = \; & \|f(\mathbf{A})\mathbf{b} - r_m(\mathbf{A})\mathbf{b} + r_m(\mathbf{A})\mathbf{b} - \mathbf{f}_m\|_{\mathbf{M}} \\ \leq \; & \|f(\mathbf{A})\mathbf{b} - r_m(\mathbf{A})\mathbf{b}\|_{\mathbf{M}} + \|\mathbf{V}_m r_m(\mathbf{A}_m)\mathbf{V}_m^H\mathbf{b} - \mathbf{V}_m f(\mathbf{A}_m)\mathbf{V}_m^H\mathbf{b}\|_{\mathbf{M}}. \end{aligned}$$

We next now bound from above each of the two terms in this sum. For the first term we use the facts that $g(\mathbf{A}) = \mathbf{M}^{-1/2} g(\mathbf{M}^{1/2}\mathbf{A}\mathbf{M}^{-1/2})\mathbf{M}^{1/2}$ for any function g such that $g(\mathbf{A})$ is a well-defined matrix function, the matrix $\mathbf{M}^{1/2}\mathbf{A}\mathbf{M}^{-1/2}$ is Hermitian and similar to $\mathbf{A}$, and $\|\mathbf{M}^{-1/2}\mathbf{x}\|_{\mathbf{M}} = \|\mathbf{x}\|_2$. We obtain

$$\begin{aligned} \|(f - r_m)(\mathbf{A})\mathbf{b}\|_{\mathbf{M}} &= \|\mathbf{M}^{-1/2}(f - r_m)(\mathbf{M}^{1/2}\mathbf{A}\mathbf{M}^{-1/2})\mathbf{M}^{1/2}\mathbf{b}\|_{\mathbf{M}} \\ &= \|(f - r_m)(\mathbf{M}^{1/2}\mathbf{A}\mathbf{M}^{-1/2})\mathbf{M}^{1/2}\mathbf{b}\|_2 \\ &\leq \|(f - r_m)(\mathbf{M}^{1/2}\mathbf{A}\mathbf{M}^{-1/2})\|_2 \|\mathbf{M}^{1/2}\mathbf{b}\|_2 \\ &= \|\mathbf{b}\|_{\mathbf{M}} \max_{\lambda\in\Lambda(\mathbf{A})} |f(\lambda) - r_m(\lambda)|. \end{aligned}$$

For the second term we obtain

$$\begin{aligned} \|\mathbf{V}_m(r_m - f)(\mathbf{A}_m)\mathbf{V}_m^H\mathbf{b}\|_{\mathbf{M}} &= \|(r_m - f)(\mathbf{A}_m)\mathbf{V}_m^H\mathbf{b}\|_2 \\ &\leq \|(r_m - f)(\mathbf{A}_m)\|_2 \|\mathbf{V}_m^H\mathbf{b}\|_2 \\ &\leq \|\mathbf{b}\|_{\mathbf{M}} \max_{\lambda\in\Lambda(\mathbf{A})} |r_m(\lambda) - f(\lambda)| \end{aligned}$$

where we have used the facts $\|\mathbf{V}_m\mathbf{x}\|_{\mathbf{M}} = \|\mathbf{x}\|_2$ and $\|\mathbf{V}_m^H\mathbf{b}\|_2 = \|\mathbf{b}\|_{\mathbf{M}}$. Adding both inequalities and noting that $\Lambda(\mathbf{A}_m)$ is contained in the spectral interval of $\mathbf{A}$, and taking the maximum over all admissible rational functions $r_m \in \mathscr{P}_{m-1}/q_{m-1}$ completes the proof.

The stated results now enable us to propose our new strategy for selecting the poles $\xi_1, \xi_2, \ldots, \xi_{m-1}$ (the zeros of q_{m-1}) for the TEM forward modeling problem.

3.1 Error Estimation Using a Surrogate Problem

The near-optimality property stated in Theorem 3.2 means that the optimization of parameters for the rational Arnoldi approximation essentially reduces to the problem of finding a denominator polynomial q_{m-1} such that the right-hand side of the error bound (22) becomes small. Note that the zeros $\xi_1, \ldots, \xi_{m-1}$ of q_{m-1} correspond to the poles used in the rational Arnoldi method for constructing a basis of the rational Krylov space. Given such a polynomial q_{m-1} and an interval $[\alpha, \beta]$, the min-max expression on the right of (22) could be computed by the Remez algorithm for uniform best approximation of f on $[\alpha, \beta]$ (see, e.g., Meinardus and Schumaker 1967). However, the computation of rational best approximants can suffer numerical instabilities and, in addition, our problem is complicated by the fact we are ultimately interested in rational approximation of parameter-dependent function $f(z) = f^t(z) = \exp(-tz)$ or $f(z) = g^\omega(z) = i\omega/(z + i\omega)$ in the time- and frequency-domain cases, respectively. We propose an alternative approach which is tailored to our problem and computationally more robust: we will estimate the min-max expression by using the rational Arnoldi method itself. For ease of exposition we first consider the problem of parameter-independent approximation of f and then introduce the parameter for f^t or g^ω later.

Given the function f and a denominator polynomial q_{m-1}, our aim is to estimate the error

$$\mathrm{err}(f, q_{m-1}) := \min_{r_m \in \mathscr{P}_{m-1}/q_{m-1}} \max_{z\in[0,+\infty]} |f(z) - r_m(z)|.$$

Note that we have formally set $[\alpha, \beta] = [0, +\infty]$ because this will allow us to obtain error bounds that are independent of the spectral interval of $\mathbf{A}$. The quantity $\max_{z\in[0,+\infty]} |f(z) - r_m(z)|$ will exist if f is bounded on $[0, +\infty]$ and q_{m-1} has no poles there; both conditions are naturally satisfied in our situation where $f = f^t$ or $f = g^\omega$, respectively.

In order to avoid the discretization of an unbounded interval we introduce the variable $\hat{z} \in [1, 2]$, the transformation $z = (\hat{z} - 1)^{-1} - 1$, the transformed function $\hat{f}(\hat{z}) = f(z)$, and the transformed denominator $\hat{q}_{m-1}(\hat{z}) = (1 - \hat{z}/\hat{\xi}_1)\cdots(1 - \hat{z}/\hat{\xi}_{m-1})$, where each $\hat{\xi}_j = (\xi_j + 1)^{-1} + 1$. Instead of the above expression for the error we now consider

$$\mathrm{err}(f, q_{m-1}) = \min_{\hat{r}_m \in \mathscr{P}_{m-1}/\hat{q}_{m-1}} \max_{\hat{z}\in[1,2]} |\hat{f}(\hat{z}) - \hat{r}_m(\hat{z})|.$$

We then use the rational Arnoldi method for approximating $\hat{f}(\widehat{\mathbf{A}})\widehat{\mathbf{b}}$ in the Euclidian inner product with a diagonal surrogate matrix $\widehat{\mathbf{A}}$ having sufficiently dense eigenvalues in $[1, 2]$, and the vector $\widehat{\mathbf{b}} = [1, \ldots, 1]^T$. Let the associated rational Arnoldi approximation be denoted as $\widehat{\mathbf{f}}_m = \hat{r}_m(\widehat{\mathbf{A}})\widehat{\mathbf{b}}$. Then by the definition of $\widehat{\mathbf{A}}$ and $\widehat{\mathbf{b}}$ we

have

$$\begin{aligned}\|\hat{f}(\widehat{\mathbf{A}})\widehat{\mathbf{b}} - \widehat{\mathbf{f}}_m\|_\infty &= \max_{\hat{\lambda}\in\Lambda(\widehat{\mathbf{A}})} |\hat{f}(\hat{\lambda}) - \hat{r}_m(\hat{\lambda})| \\ &\le \max_{\hat{z}\in[1,2]} |\hat{f}(\hat{z}) - \hat{r}_m(\hat{z})| \qquad (23) \\ &= \mathrm{err}(f, q_{m-1}),\end{aligned}$$

where the expression on the left-hand side is easy to compute as $\hat{f}(\widehat{\mathbf{A}})\widehat{\mathbf{b}}$ is explicitly known (a function of a diagonal matrix is the diagonal matrix of the function values). Note that building a rational Krylov basis with $\widehat{\mathbf{A}}$ is computationally inexpensive as we only need to solve linear systems with a diagonal matrix.

As becomes clear from (23) we can only compute a lower bound for $\mathrm{err}(f, q_{m-1})$ with the described procedure. However, the inequality in (23) can be expected to be sufficiently sharp if $\Lambda(\widehat{\mathbf{A}})$ is a sufficiently dense discretization of $[1, 2]$, so that "spectral adaptation" in the rational Arnoldi method does not yet occur (which means that the method behaves as if the spectrum of $\widehat{\mathbf{A}}$ were a continuum). A detailed analysis of spectral adaptation in the rational Arnoldi method is given in Beckermann, Güttel, and Vandebril (2010) and Beckermann and Güttel (2012), where it is shown that the region of "deflated eigenvalues" depends on the ratio $m/\widehat{N}$, that is, the number of rational Arnoldi iterations m compared to the size $\widehat{N}$ of the surrogate matrix $\widehat{\mathbf{A}}$. For all numerical results reported below, specifically in Table 1, we have used $m \le 72$ and found that, with a diagonal matrix $\widehat{\mathbf{A}}$ with $\widehat{N} = 3000$ equidistant eigenvalues in the interval $[1, 2]$, no noticeable spectral adaptation occurred. A further increase of $\widehat{N}$ did not change the results in any digit reported in Table 1.

We remark that more elaborate strategies for choosing $\widehat{N}$ and the eigenvalues of the surrogate $\widehat{\mathbf{A}}$ could be motivated by the interpolation characterization in Theorem 3.1. For example, one could start with a small number of $\widehat{N}_1 = 2m$ equispaced eigenvalues and then refine the spectrum to $\widehat{N}_2, \widehat{N}_3, \ldots$ eigenvalues by adding geometric means of rational Ritz values. We have not implemented such a strategy here as the pole optimization is a one-time calculation requiring negligible computing time compared to the solution of the forward modeling problem.

3.2 Pole Optimization

As we shall argue below that there is no advantage to performing the forward modeling in the frequency domain, we shall restrict the following discussion to the time-domain case where $f(z) = f^t(z) = e^{-tz}$.

Now that $\mathrm{err}(f, q_{m-1})$ can be estimated efficiently for a given q_{m-1} and any function $f = f^t$ (all Arnoldi approximants $\widehat{\mathbf{f}^t_m}$ for $f^t(\widehat{\mathbf{A}})\widehat{\mathbf{b}}$ can be extracted from the same rational Krylov space), it remains to find a fixed "optimal" q_{m-1} which minimizes $\mathrm{err}(f^t, q_{m-1})$ uniformly for all parameters $t \in [t_{\min}, t_{\max}]$. This is a constrained nonlinear optimization problem:

(P0) Find $q_{m-1}(z) = \prod_{j=1}^{m-1}(1 - z/\xi_j)$ such that

$$\max_{t\in[t_{\min},t_{\max}]} \mathrm{err}(f^t, q_{m-1}) \approx \max_{t\in[t_{\min},t_{\max}]} \|\hat{f}^t(\widehat{\mathbf{A}})\widehat{\mathbf{b}} - \widehat{\mathbf{f}}^t_m\|_\infty$$

is minimal, with the constraint that the poles ξ_j be negative.

To enable the efficient solution of this problem we have applied two further constraints. First, we assume that $m - 1$ is divisible by an integer $\ell < m$ and $q_{m-1}(z)$ is factored in the form

$$q_{m-1}(z) = (1-z/\xi_1)^{(m-1)/\ell}(1-z/\xi_2)^{(m-1)/\ell}\cdots(1-z/\xi_\ell)^{(m-1)/\ell}.$$

This reduces the problem of finding $m - 1$ parameters to that of finding merely ℓ parameters. Recall again that the poles $\xi_1, \ldots, \xi_\ell$ correspond to shifts in linear system solves, so reusing these shifts for $(m - 1)/\ell$ rational Arnoldi iterations is also convenient when direct solvers are employed. Note, however, that this constraint on the factorization of q_{m-1} leads to the somewhat counter-intuitive effect that, for m constant, the error $\mathrm{err}(f^t, q_{m-1})$ may slightly increase as the number of distinct parameters ℓ increases (see, for example, Table 1).

Second, for $f^t = \exp(-tz)$ we can restrict the set of admissible poles further by using a result of Andersson 1981, which states that the best uniform rational approximant $r_{m-1}(z)$ of type $(m - 1, m - 1)$ with negative poles that minimizes $\max_{z\in[0,\infty]} |\exp(-z) - r_{m-1}(z)|$ is of the form $p_{m-1}(z)/(1 - z/\xi)^{m-1}$, i.e., all poles are concentrated at $\xi < 0$. Moreover, by scaling z to tz we find that the best uniform rational approximant $r_{m-1}(z)$ of type $(m - 1, m - 1)$ with negative poles that minimizes $\max_{z\in[0,\infty]} |\exp(-tz) - r_{m-1}(z)|$ is of the form $p_{m-1}(z)/(1 - tz/\xi)^{m-1}$ with some polynomial $p_{m-1} \in \mathscr{P}_{m-1}$, i.e., all poles are concentrated at $t\xi < 0$. It is therefore reasonable to restrict the poles $\xi_1, \ldots, \xi_\ell$ for uniform approximation of $f^t(z) = \exp(-tz)$ with $t \in [t_{\min}, t_{\max}]$ to the interval $[\xi_{\min}, \xi_{\max}]$, where $\xi_{\min} < 0$ is the optimal concentrated pole of the rational approximant $p_{m-1}(z)/(1 - tz/\xi_{\min})^{m-1}$ for $\exp(-t_{\min} z)$, and $\xi_{\max} = \xi_{\min} t_{\min}/t_{\max}$.

To summarize, we arrived at the following optimization problem:

(P1) Find $q_{m-1}(z) = \prod_{j=1}^{\ell}(1 - z/\xi_j)$ such that

$$\max_{t\in[t_{\min},t_{\max}]} \mathrm{err}(f^t, q_{m-1}) \approx \max_{t\in[t_{\min},t_{\max}]} \|\hat{f}^t(\widehat{\mathbf{A}})\widehat{\mathbf{b}} - \widehat{\mathbf{f}}^t_m\|_\infty$$

is minimal, with the constraint being that all $\xi_j \in [\xi_{\min}, \xi_{\max}]$.

We have used MATLAB to solve this minimization problem for the time interval $[t_{\min}, t_{\max}] = [10^{-6}, 10^{-3}]$, with $m - 1 = 12, 24, \ldots, 72$ and $\ell = 1, 2, 3, 4$. As this problem seems to have many local minima, we determined the parameters $\xi_1, \ldots, \xi_\ell$ by first performing a global search on a coarse discretization of $[\xi_{\min}, \xi_{\max}]$ with 100 logarithmically equispaced points, and then refining the result using MATLAB's `fmincon` routine. The surrogate problem was of size $\widehat{N} = 3000$. The results are reported in Table 1.

This table can be used in the following way: if no parallel solution of linear systems is desired, Table 1 reveals that it is most efficient to use two cyclically repeated poles. To determine the optimal poles for a time interval of, say, $[10^{-6}, 10^{-3}]$, one reads off the two poles in the first row for which the desired level of accuracy is reached. The first column of this row then gives the number required rational Krylov iterations $(m - 1)$ (the resulting rational Krylov space is of dimension m). For example, to achieve an error level below 10^{-7} it is sufficient to run $m - 1 = 36$ rational Krylov iterations and repeat the two poles $\xi_1 = -3.32e + 4$ and $\xi_2 = -3.88e + 06$ cyclically 18 times. By the scaling argument given above, the table can also be used for other time intervals consisting of 3 decades. For the time interval $[10^{-5}, 10^{-2}]$, for example, the poles have to be relaced by $\xi_1/10$ and $\xi_2/10$.

[Table 1 about here.]

The poles in Table 1 have been optimized to give a uniform approximation over a time interval. We note that it is also easily possible to optimize the poles with respect to a positive weight function

$w(t)$ by minimizing $\max_{t\in[t_{\min},t_{\max}]} w(t)\cdot \mathrm{err}(f^t, q_{m-1})$. This can be used to improve the approximation in certain parts of the time interval, such as for late times, particularly when the asymptotic behavior of the transient is known from analytic solutions (cf. Ward and Hohmann (1987)).

3.3 Relation to Existing Work and Other Pole Selection Strategies

In this section we briefly review some other pole selection strategies. For a more detailed survey we refer to Güttel 2013.

The problem of optimizing a single repeated negative pole for approximating $\exp(-t_0\mathbf{A})\boldsymbol{b}$ for a single time point t_0 was considered in Eshof and Hochbruck 2006. In case of a single pole the corresponding rational approximation problem can be transformed into an equivalent polynomial approximation problem, and this problem can be solved numerically using the Remez algorithm Eshof and Hochbruck 2006. Our problem of uniform approximation on a time interval $[t_{\min}, t_{\max}]$ can be seen as a generalization, but in the case of two or more cyclically repeated poles it does not seem to be possible to find an equivalent polynomial formulation. A result bounding the error of rational Arnoldi approximants with cyclically repeated poles in terms of the error of single pole approximants was given in Güttel 2010, p. 113–115.

A different route of computing poles asymptotically optimal for all $t > 0$ was followed in V. L. Druskin, Knizhnerman, and Zaslavsky 2009. Here the constructed negative poles are given in terms of elliptic functions and it is shown that the rational Arnoldi method with these parameters will converge with a geometric rate given by

$$\limsup_{m\to\infty} \|\exp(-t\mathbf{A})\mathbf{b}-\mathbf{f}_m^t\|^{1/m} \simeq \exp\left(-\frac{\pi^2}{4\log(2/\delta)}\right), \quad \text{for all } t>0, \tag{24}$$

where $\mu = \left(\frac{1-\delta}{1+\delta}\right)^2$ and $\delta = \sqrt{\frac{\lambda_{\min}}{\lambda_{\max}}}$, with $\lambda_{\max}$ and $\lambda_{\min}$ denoting the largest and smallest nonzero eigenvalue of $\mathbf{A}$, respectively. Note that the convergence rate on the right of (24) deteriorates with a growing condition number $\lambda_{\max}/\lambda_{\min}$ of $\mathbf{A}$, hence this approach cannot be expected to give convergence independent of mesh or conductivity structure. On the other hand, the rate is independent of the length of the time interval $[t_{\min}, t_{\max}]$, so this approach becomes favourable when the condition number of $\mathbf{A}$ is moderate and $[t_{\min}, t_{\max}]$ is a very large interval. See V. Druskin, Lieberman, et al. 2010 for an adaptive version of this pole selection approach. We end by remarking that these asymptotically optimal pole sequences consist of pairwise distinct poles, so no factorizations of shifted matrices can be reused in the rational Arnoldi method when a direct solver is employed.

3.4 Relation Between Frequency and Time Domain Approaches

We have discussed an approach for approximating the transient of the TEM solution directly in time domain. However, as mentioned in Section 1, an alternative approach is to synthesize the time-domain solution from frequency-domain solutions by computing the inverse Fourier transform (10). The latter can be efficiently approximated numerically to desired accuracy by fast Hankel transform (FHT) techniques as described in Johansen and Sørensen (1979) and refined in Christensen (1990), where also bounds on the number of frequency-domain solutions required for a sufficiently accurate transient can be found. By using rational Krylov subspace approximation in the frequency domain a uniformly accurate solution approximation $\mathbf{u}(\omega)$ is available for all frequencies as soon as a Krylov subspace of sufficiently large dimension has been constructed (cf. Börner et al. (2008)). As a consequence, considerably fewer frequency-domain problems need to be solved than necessary to obtain an accurate transient via the FHT.

In both the time and frequency domains the rational Krylov spaces are constructed using the same matrix $\mathbf{A}$ and initial vector $\mathbf{b}$, but may differ in the pole sequence, which should be chosen in an optimal fashion for the function g^ω in the frequency domain and f^t in the time domain. We argue that the frequency domain approximation followed by FHT cannot yield a significantly better approximation than that obtained in the time domain: the FHT results in a time domain approximation which is a linear combination of vectors from the frequency domain Krylov space. One could then, using the same poles as in the frequency domain, construct a rational Krylov approximation of $f^t(\mathbf{A})\mathbf{b}$, and the near-optimality of the rational Krylov approximation (see Theorem 3.2) would select an approximation which is at least as good as the FHT-transformed frequency domain approximation. Using poles in the time domain which are chosen in an optimal fashion for the function f^t would only further improve this approximation. For this reason we restrict ourselves to time-domain examples in the following section.

4 NUMERICAL EXPERIMENTS

We present a series of numerical experiments for two model problems to illustrate the important features of the rational Arnoldi approximation of TEM in the time and frequency domains. In the first set we consider the transient response of a vertical magnetic dipole located atop a layered half-space. For this model problem there is a closed-form solution available (see Ward and Hohmann 1987), which can be used as a reference solution to analyze the contributions of the errors due to the boundary condition, the finite element discretization and the rational Arnoldi approximation. We are able to verify that the convergence of the rational Arnoldi approximation is uniform in both time and frequency.

A model with terrain topography serves as a second numerical example. We demonstrate that models incorporating surface topography can be modeled without additional numerical effort. In the past, the inclusion of the air half-space has often been avoided due to specific limitations of the involved time integration methods. More specifically, all variants of the explicit Euler method, e.g., the DuFort-Frankel method, require small time steps which are bounded by the square root of the lowest electrical conductivity within the model. Typical values for the choice of the air half-space conductivity range between 10^{-14} and 10^{-6} S/m. Polynomial Krylov methods generally require more iterations when the air layer is included in the discretization. In view of these limitations it has often been desired to exclude the air layer from the computational domain (Oristaglio and Hohmann 1984; Y. Goldman, Hubans, et al. 1986; Y. Goldman, Joly, et al. 1989; Wang and Hohmann 1993). However, the physical effect of the insulating air layer on the electric field and its spatial derivative normal to this plane can be expressed by a boundary condition imposed at the Earth's surface. This boundary condition is non-local, i.e., it incorporates all degrees of freedom associated with tetrahedron faces adjacent with this boundary. To express the boundary condition at a single point at this plane, a convolution type integral has to be assembled and incorporated into the discretized curl-curl operator as a dense block matrix. Hence, the numerical effort for the compu-

tation of transients with a non-local boundary condition exhibits a significantly lower efficiency due to the increased memory requirements. This poses a limit on the speed of the linear system solves which form the numerical kernel of rational Krylov methods.

4.1 Layered Half-Space

We first consider the model of a layered half-space. A layer with an electrical resistivity of $30\,\Omega\cdot\mathrm{m}$ and a thickness of 30 m is embedded in a homogeneous half-space of $100\,\Omega\cdot\mathrm{m}$ at a depth of 100 m. A vertical magnetic dipole source is approximated by a small $10\times 10\,\mathrm{m}^2$ horizontal loop located at the Earth's surface, i.e., at $z=0$.

The computational domain Ω consists of a cube of side length 2 km centered at the origin, which is also the center of the square transmitter coil. We used the mesh generator of the COMSOL finite element package (Version 3.5a) to generate a tetrahedral mesh. By making the line segments which form the transmitter coil sufficiently small and fixing a sufficiently small maximal element size in the vicinity of the observation point, a local refinement of the mesh near transmitter and receiver was achieved. Fig. 1 shows the trace of the tetrahedral mesh looking down on the surface $z=0$, where the local refinement in the vicinity of the dipole source is visible. The mesh employed for the computations consists of 24,582 tetrahedra. The matrices $\mathbf{M}$ and $\mathbf{C}$ in the time- and frequency-domain discretizations (13) and (14) have dimensions $N=27,623$ and $N=152,078$ for the Nédélec spaces of order $k=1$ and $k=2$, respectively.

Fig. 2 shows the decrease of the relative error to the true discrete transient measured in the $\|\cdot\|_{\mathbf{M}}$-norm against the number of rational Arnoldi iterations for spatial discretization with Nédélec elements of order $k=1$ (left column) and $k=2$ (right column), each using one, two and three cyclically repeated poles in the rational Arnoldi method (rows one, two and three). The poles were optimized for a Krylov space of dimension 36 (cf. Tab. 1). Each line corresponds to the transient of the electric field at for a discrete set of times between $t=10^{-6}$s to 10^{-3}s. The dashed black line denotes the error level guaranteed uniformly for all times by the number of poles according to Table 1, which are clearly seen to be achieved. As one can observe both from Table 1 as well as Fig. 2, using three (or four) poles does not result in a further error decrease after $m=37$ Arnoldi iterations compared to using only two cyclically repeated poles. However, using a higher number of cyclically repeated poles offers more potential for parallel solution of the linear systems as mentioned in Section 1.

For the purpose of comparison a frequency domain-based solution was computed in addition to the time domain approximation via the rational Arnoldi method. To eliminate the error of applying the rational Arnoldi method in the frequency-domain, we computed the frequency domain solutions directly at all frequencies required by the FHT in order to obtain a sufficiently accurate transient. In the following, we refer to this approximation as the *brute force frequency-domain solution*, which differs from the analytical solution only by the spatial finite element discretization error. Fig. 3 shows, for a first-order Nédélec discretization in space, a comparison of the accuracy of the transient evaluated at $\boldsymbol{x}=(100,0,0)$ obtained for a rational Arnoldi approximation using Krylov spaces of dimension $m=13$ (left column) and $m=73$ (right column) based on one, two and three cyclically repeated poles (rows one, two and three), against the analytical solution (black line) and the brute force frequency domain approximation (green line). It can be observed that an approximation essentially indistinguishable from the brute force approximation is achieved already for $m=13$. The difference to the analytical solution is due to the spatial resolution, which is improved in the analogous plots in Fig. 4 for a second-order Nédélec discretization based on the same mesh. Here we observe that a larger Krylov space is necessary for the Arnoldi error to reach the level of discretization error. Fig. 5 gives the error of the transient against simulation time for Krylov spaces of different dimensions for first (left column) and second (right column) order Nédélec discretization. A summary of run times is given in Fig. 6, where we observe the quadratic dependence on the Krylov space dimension m with a higher constant for second-order Nédélec elements.

For the construction of the rational Arnoldi basis we have used one, two, and three poles which have been repeated $1,2,\ldots,6$ times, thus yielding a rational Krylov space with $m-1=12,24,\ldots,72$. The appropriate poles are listed in Tab. 1. The numerical effort is dominated by the number of LU factorization steps necessary (one for each pole), and one additional LU factorization for the evaluation of the vector $\mathbf{b}=\mathbf{M}^{-1}\mathbf{q}$. Even though a linear system with $\mathbf{A}$ has to be solved in each Arnoldi iteration, the cyclic repetition of the poles yields a remarkable saving in computational time (Tab. 2).

[Table 2 about here.]

[Figure 1 about here.]

[Figure 2 about here.]

[Figure 3 about here.]

[Figure 4 about here.]

[Figure 5 about here.]

[Figure 6 about here.]

4.2 Homogeneous Subsurface with Topography

As outlined above, our proposed pole selection method yields rational Arnoldi approximations which exhibit a uniform convergence that is independent of the properties of the underlying spatial discretization. Therefore, it seems attractive to include the air layer in the computational domain, which allows for the modeling of topography. The use of finite elements for the spatial discretization further adds to this benefit, as it allows for greater flexibility in approximating a curved air-Earth interface. We demonstrate this by computing transients generated by a vertical magnetic dipole source laid out atop a homogeneous half-space in the vicinity of a morphological hill-shaped feature. The interface between the air and the conducting half-space shows a moderate morphology accentuated at the center of the plane $z=0$ around $x=y=0$ m. The hill has a height of 38 m and a circular shape with a diameter of approximately 200 m (Fig. 7). At large distance from the hill, the interface between air and Earth is a horizontal plane aligned with $z=0$. Fig. 7 shows the trace of the tetrahedral mesh from various azimuth and elevation angles. A comparison of transients $\partial_t B_z$ measured at the plane $y=0$ at the points $x=[-10,0,130,270]$ m and $z=[0,38,0,0]$ m are plotted in Fig. 8. A distinct distortion of the transient signal is visible at early times in the vicinity of the hill. Snapshots of the magnitude of the horizontal component of the induced electrical current system $\boldsymbol{J}$ in $\mathrm{A}\cdot\mathrm{m}^{-2}$ across the plane $y=0$ are given in Fig. 9 for times $t=[10^{-6},10^{-5},10^{-4}]$ s.

[Table 3 about here.]

Tables 2 and 3 give a breakdown of the run times required for the different phases of the solution process for both numerical test cases. The computations were carried out in MATLAB R2012b pinned to 8 cores of an Intel Xeon E5-4620 (Sandy Bridge) system (2.2 GHz). For the direct sparse linear solves we employed the PARDISO solver (Schenk and Gärtner 2004) as contained in the Intel MKL. It can be observed that the computation of the rational Arnoldi approximant using formula (21) is negligible compared to the construction of the rational Arnoldi decomposition (20). The resulting run time is still far below the brute force approximation in which all frequency domain solutions required for the FHT transformation to the time domain are computed by solving a full finite element system.

[Figure 7 about here.]

[Figure 8 about here.]

[Figure 9 about here.]

5 CONCLUSIONS

We have presented a computational method for 3-D transient electromagnetic forward modeling based on Nédélec finite element discretization in space and rational Krylov subspace approximation for the time integration. Once the finite element discretization in space is given, the method requires only the selection of a small number of cyclically repeated poles which parametrize the rational Arnoldi method. These poles can be obtained from Table 1 depending on the desired accuracy or, if sparse direct solvers are to be employed for the finite element systems in parallel, on the available level of parallelism. The attractive features of our rational Arnoldi method is the uniform accuracy in time independent of spatial mesh width or conductivity structure. Moreover, the cyclic reuse of a small number of poles allows the amortization of a small number of matrix factorizations over the generation of the rational Krylov space. This represents an advantage over previously proposed pole sequences which are not mesh independent and require a new matrix factorization at every Krylov iteration. If iterative methods are used to solve the finite element systems an added benefit is that the poles as given in Table 1 lie well separated from the origin, suggesting that the resulting shifted linear systems are well-conditioned. By expressing the time and frequency domain problems in terms of matrix functions we have emphasized both the relationship of the two formulations as well as how both can be solved using rational Krylov subspace approximation.

References

Andersson, J.-E. (1981). Approximation of e^{-x} by rational functions with concentrated negative poles. English. *J. Approx. Theory* **32**, 85–95. DOI: 10.1016/0021-9045(81)90106-4.

Beckermann, B., Güttel, S., and Vandebril, R. (2010). On the convergence of rational Ritz values. *SIAM J. Matrix Anal. Appl.* **31**, 1740–1774.

Beckermann, B. and Reichel, L. (2009). Error estimation and evaluation of matrix functions via the Faber transform. *SIAM J. Numer. Anal.* **47**, 3849–3883.

Beckermann, B. and Güttel, S. (2012). Superlinear convergence of the rational Arnoldi method for the approximation of matrix functions. *Numerische Mathematik* **121**(2), 205–236.

Börner, R.-U., Ernst, O. G., and Spitzer, K. (2008). Fast 3D simulation of transient electromagnetic fields by model reduction in the frequency domain using Krylov subspace projection. *Geophys. J. Int.* **173**, 766–780.

Christensen, N. B. (1990). Optimized Fast Hankel Transform Filters. *Geophysical Prospecting* **38**, 545–568.

Commer, M. and Newman, G. (2004). A parallel finite-difference approach for 3D transient electromagnetic modeling with galvanic sources. *Geophysics* **69**(5), 1192–1202. URL: http://link.aip.org/link/?GPY/69/1192/1.

Druskin, V. L., Knizhnerman, L. A., and Zaslavsky, M. (2009). Solution of large scale evolutionary problems using rational Krylov subspaces with optimized shifts. *SIAM J. Sci. Comput.* **31**, 3760–3780.

Druskin, V. L. and Knizhnerman, L. A. (1988). Spectral Differential-Difference Method for Numeric Solution of Three-Dimensional Nonstationary Problems of Electric Prospecting. *Izvestiya, Earth Physics* **24**(8), 641–648.

— (1994). Spectral approach to solving three-dimensional Maxwell's diffusion equations in the time and frequency domains. *Radio Science* **29**(4), 937–953.

Druskin, V. L., Knizhnerman, L. A., and Lee, P. (1999). New Spectral Lanczos Decomposition Method for Induction Modeling in Arbitrary 3-D Geometry. *Geophysics* **64**(3), 701–706.

Druskin, V. L. and Simoncini, V. (2011). Adaptive Rational Krylov Spaces for Large-Scale Dynamical Systems. *Systems & Control Letters* **60**, 546–560.

Druskin, V., Lieberman, C., and Zaslavsky, M. (2010). On Adaptive Choice of Shifts in Rational Krylov Subspace Reduction of Evolutionary Problems. *SIAM J. Sci. Comput.* **32**(5), 2485–2496.

Druskin, V., Remis, R., and Zaslavsky, M. (2014). An Extended Krylov Subspace Model-Order Reduction Technique to Simulate Wave Propagation in Unbounded Domains. *arXiv preprint arXiv:1402.7090*.

Druskin, V. and Zaslavsky, M. (2011). On convergence of Krylov subspace approximations of time-invariant self-adjoint dynamical systems. *Linear Algebra Appl.*

DuFort, E. C. and Frankel, S. P. (1953). Stability conditions in the numerical treatment of parabolic differential equations. *Math. tables and other aids to comput. (former title of Math. Comput.)* **7**, 135–152.

Ericsson, T. (1990). *Computing functions of matrices using Krylov subspace methods*. Technical report. Department of Computer Science, Chalmers University of Technology and the University of Göteborg.

Eshof, J. and Hochbruck, M. (2006). Preconditioning Lanczos approximations to the matrix exponential. English. *SIAM J. Sci. Comput.* **27**, 1438–1457. DOI: 10.1137/040605461.

Goldman, M. M. and Stoyer, C. H. (1983). Finite-difference calculations of the transient field of an axially symmetric earth for vertical magnetic dipole excitation. *Geophysics* **48**, 953–963.

Goldman, Y., Hubans, C., Nicoletis, S., and Spitz, S. (1986). A finite-element solution for the transient electromagnetic response of an arbitrary two-dimensional resistivity distribution. *Geophysics* **51**, 1450–1461.

Goldman, Y., Joly, P., and Kern, M. (1989). The Electric Field in the Conductive Half Space as a Model in Mining and Petroleum Engineering. *Math. Meth. Appl. Sci.* **11**, 373–401.

Gopalakrishnan, J., Garcia-Castillo, L. E., and Demkowicz, L. F. (2005). Nédélec Elements in Affine Coordinates. *Computers and Mathematics with Applications* **49**, 1285–1294.

Güttel, S. (2010). "Rational Krylov Methods for Operator Functions". PhD thesis. TU Bergakademie Freiberg.

— (2013). Rational Krylov approximation of matrix functions: Numerical methods and optimal pole selection. *GAMM Mitt.* **36**(1), 8–31.

Haber, E., Ascher, U., Oldenburg, D. W., et al. (2002). 3D forward modelling of time domain electromagnetic data. *2002 SEG Annual Meeting*. Society of Exploration Geophysicists.

Johansen, H. K. and Sørensen, K. (1979). Fast Hankel Transforms. *Geophysical Prospecting* **27**(4), 876–901.

Kirby, R. C. (2014). Low-Complexity Finite Element Algorithms for the De Rham Complex on Simplices. *SIAM J. Sci. Comput.* **36**(2), A846–A868.

Knizhnerman, L. A., Druskin, V. L., and Zaslavsky, M. (2009). On optimal convergence rate of the rational Krylov subspace reduction for electromagnetic problems in unbounded domains. *SIAM J. Numer. Anal.* **47**, 953–971.

Meinardus, G. and Schumaker, L. L. (1967). Approximation of functions: Theory and numerical methods. Springer.

Monk, P. (2003). Finite Element Methods for Maxwell's Equations. Oxford University Press.

Mulder, W. A., Wirianto, M., and Slob, E. C. (2008). Time-domain modeling of electromagnetic diffusion with a frequency-domain code. *Geophysics* **73**(1), F1–F8.

Newman, G. A., Hohmann, G. W., and Anderson, W. L. (1986). Transient electromagnetic response of a three-dimensional body in a layered earth. *Geophysics* **51**, 1608–1627.

Oristaglio, M. L. and Hohmann, G. W. (1984). Diffusion of electromagnetic fields into a two-dimensional earth: A finite-difference approach. *Geophysics* **49**, 870–894.

Ruhe, A. (1994a). Rational Krylov algorithms for nonsymmetric eigenvalue problems. *IMA Vol. Math. Appl.* **60**, 149–164.

— (1994b). Rational Krylov algorithms for nonsymmetric eigenvalue problems. II: Matrix pairs. English. *Linear Algebra Appl.* **197/198**, 283–296. DOI: 10.1016/0024-3795(94)90492-8.

Saad, Y. (1992). Analysis of Some Krylov Subspace Approximations to the Exponential Operator. *SIAM J. Numer. Anal.* **29**, 209–228.

Schenk, O. and Gärtner, K. (2004). Solving Unsymmetric Sparse Systems of Linear Equations with PARDISO. *Future Gener. Comp. Systems* **20**, 475–487.

Taflove, A. (1995). Computational Electrodynamics: The Finite-Difference Time-Domain Method. Norwoord, MA: Artech House.

Wang, T. and Hohmann, G. W. (1993). A finite-difference, time-domain solution for three-dimensional electromagnetic modelling. *Geophysics* **58**(6), 797–809.

Ward, S. H. and Hohmann, G. W. (1987). "Electromagnetic Theory for Geophysical Applications". *Electromagnetic Methods in Applied Geophysics*. Edited by M. N. Nabighian. Volume 1. Soc. Expl. Geophys. Chapter 4, pages 131–311.

Yee, K. S. (1966). Numerical solution of initial boundary value problems involving Maxwell's equations in isotropic media. *IEEE Trans. Antennas Propag.* **AP-14**, 302–307.

Zaslavsky, M., Druskin, V. L., and Knizhnerman, L. A. (2011). Solution of 3D time-domain electromagnetic problems using optimal subspace projection. *Geophysics* **76**(6), F339–F3351.

LIST OF FIGURES

(a)

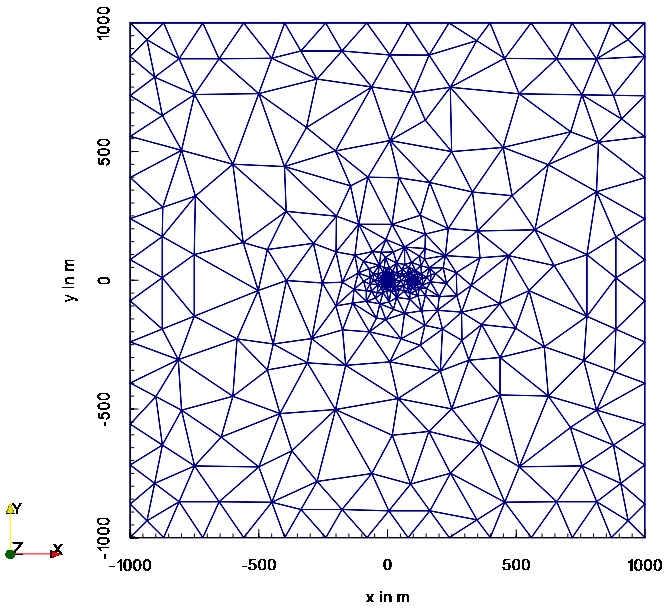

(b)

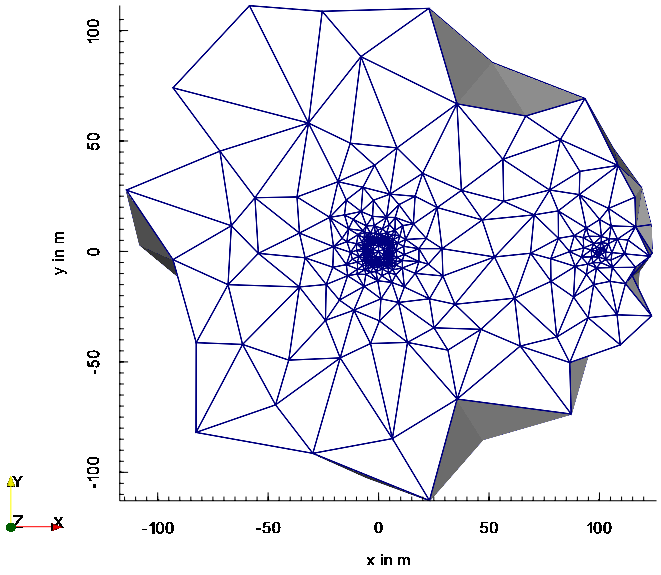

Figure 1. Trace of the tetrahedral finite element mesh on the plane $z = 0$ (a). Panel (b) zooms into the area of transmitter and receiver. The air layer, which has a thickness of 1000 m, has been omitted in the plots.

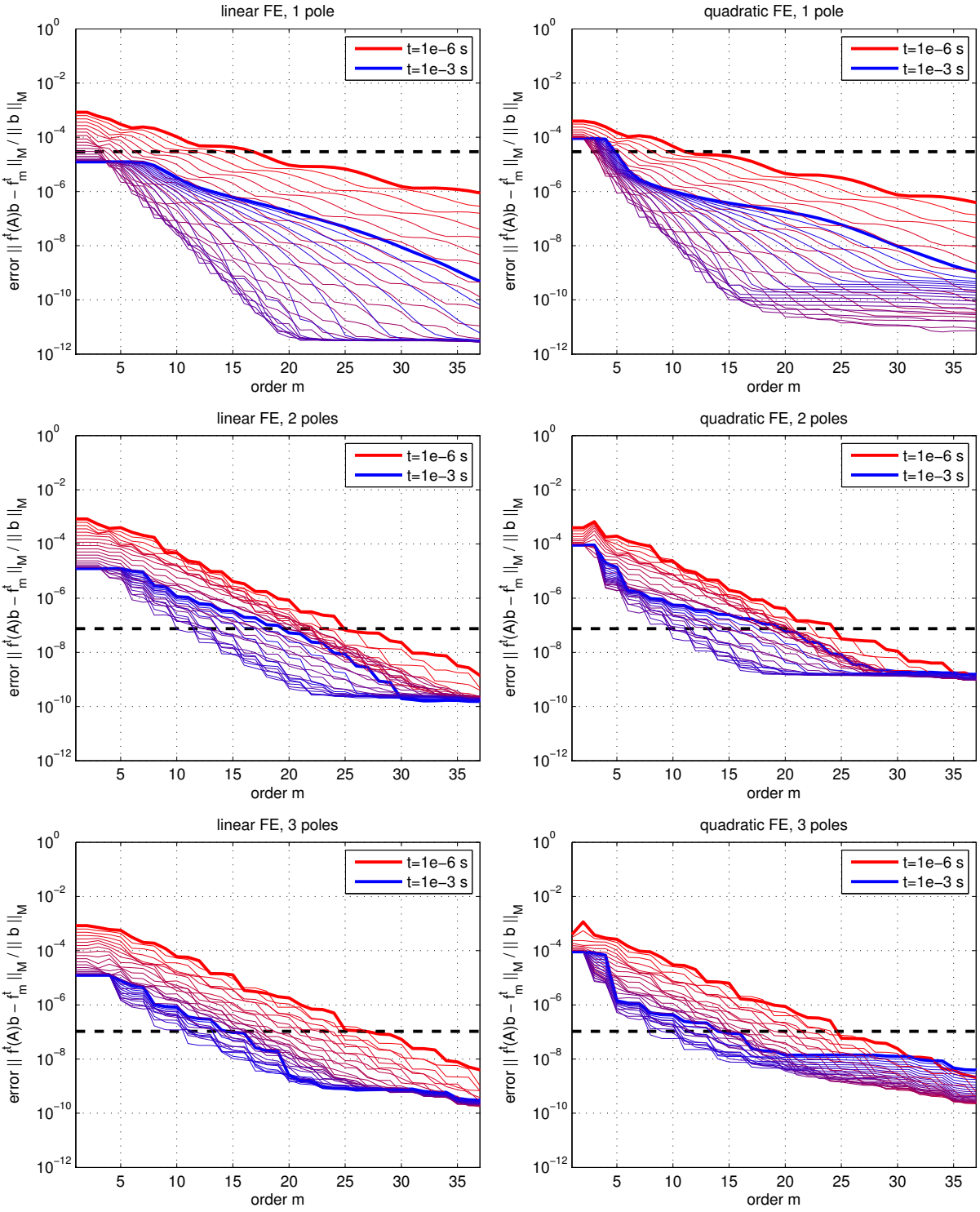

Figure 2. Errors of the rational Arnoldi approximations of dimension $m = 1, 2, \ldots, 37$ with respect to a higher order rational Arnoldi approximation ($m = 42$) for all desired times $t \in [10^{-6} \ldots 10^{-3}]$ s, where the poles used are those optimized for $m - 1 = 36$.

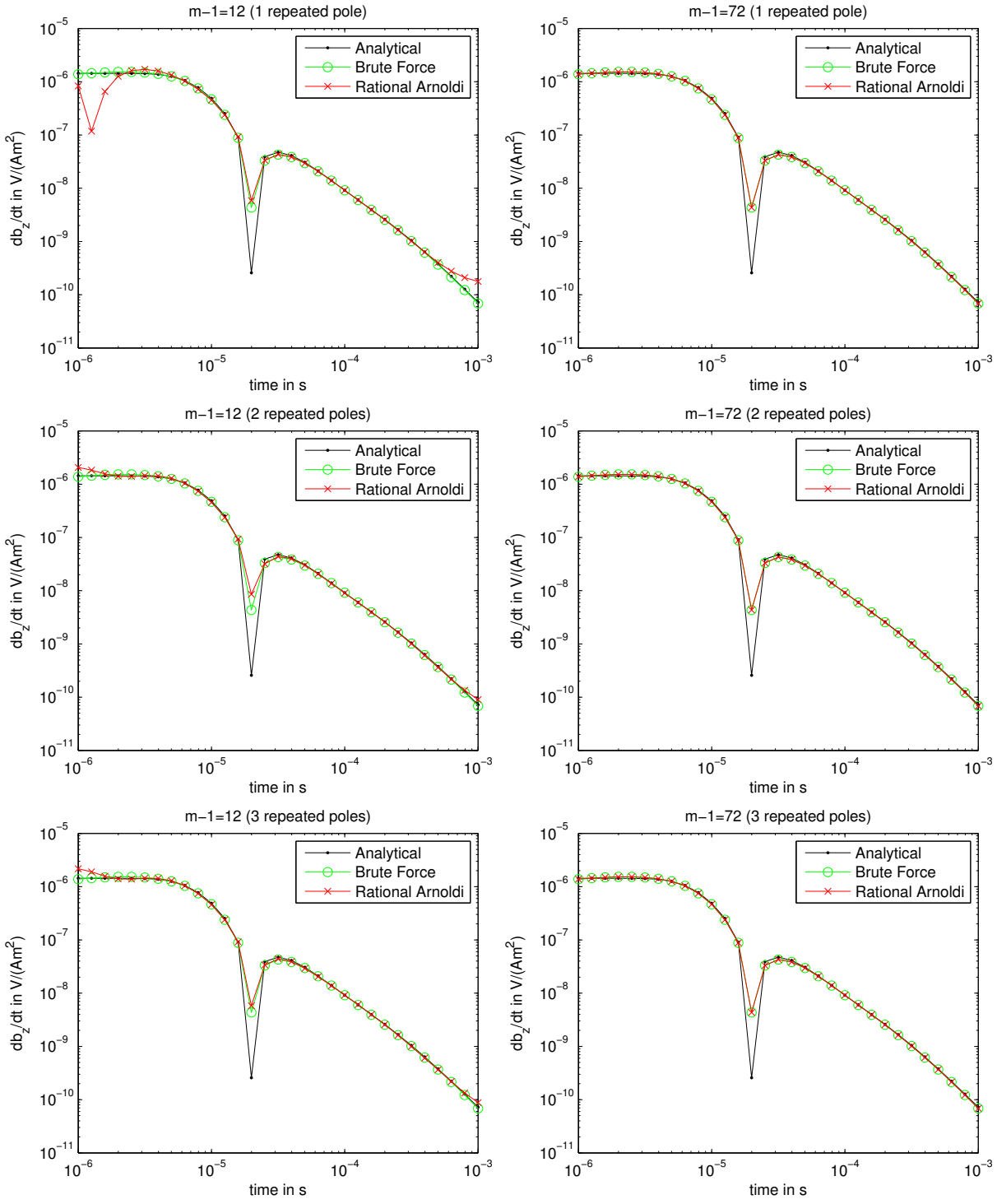

Figure 3. Comparison of transients $\partial_t B_z$ evaluated at $\boldsymbol{x} = (100, 0, 0)$ m extracted from a rational Arnoldi approximation of order $m = 13$ and $m = 73$ (left and right columns, resp.) using 1, 2, and 3 cyclically repeated poles (top, middle, and bottom row, resp.) with an analytical solution, and the brute force solution obtained by inverse Fourier transform of frequency-domain solutions (14) for the layered half-space model. Nédélec FE of order $k = 1$.

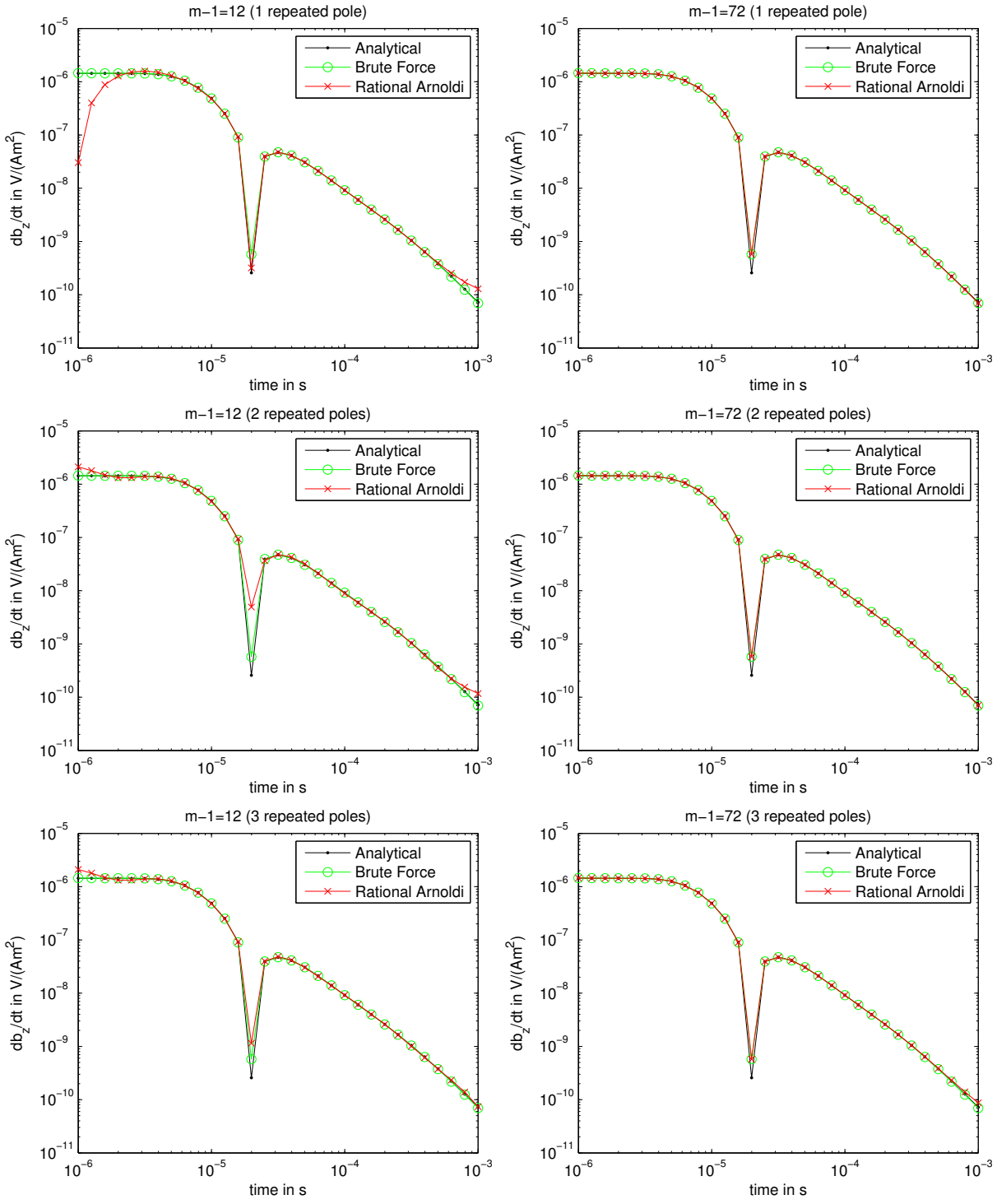

Figure 4. Comparison of transients $\partial_t B_z$ evaluated at $\boldsymbol{x} = (100, 0, 0)$ m extracted from a rational Arnoldi approximation of order $m = 13$ and $m = 73$ (left and right columns, resp.) using 1, 2, and 3 cyclically repeated poles (top, middle, and bottom row, resp.) with an analytical solution, and the brute force solution obtained by inverse Fourier transform of frequency-domain solutions (14) for the layered half-space model. Nédélec FE of order $k = 2$.

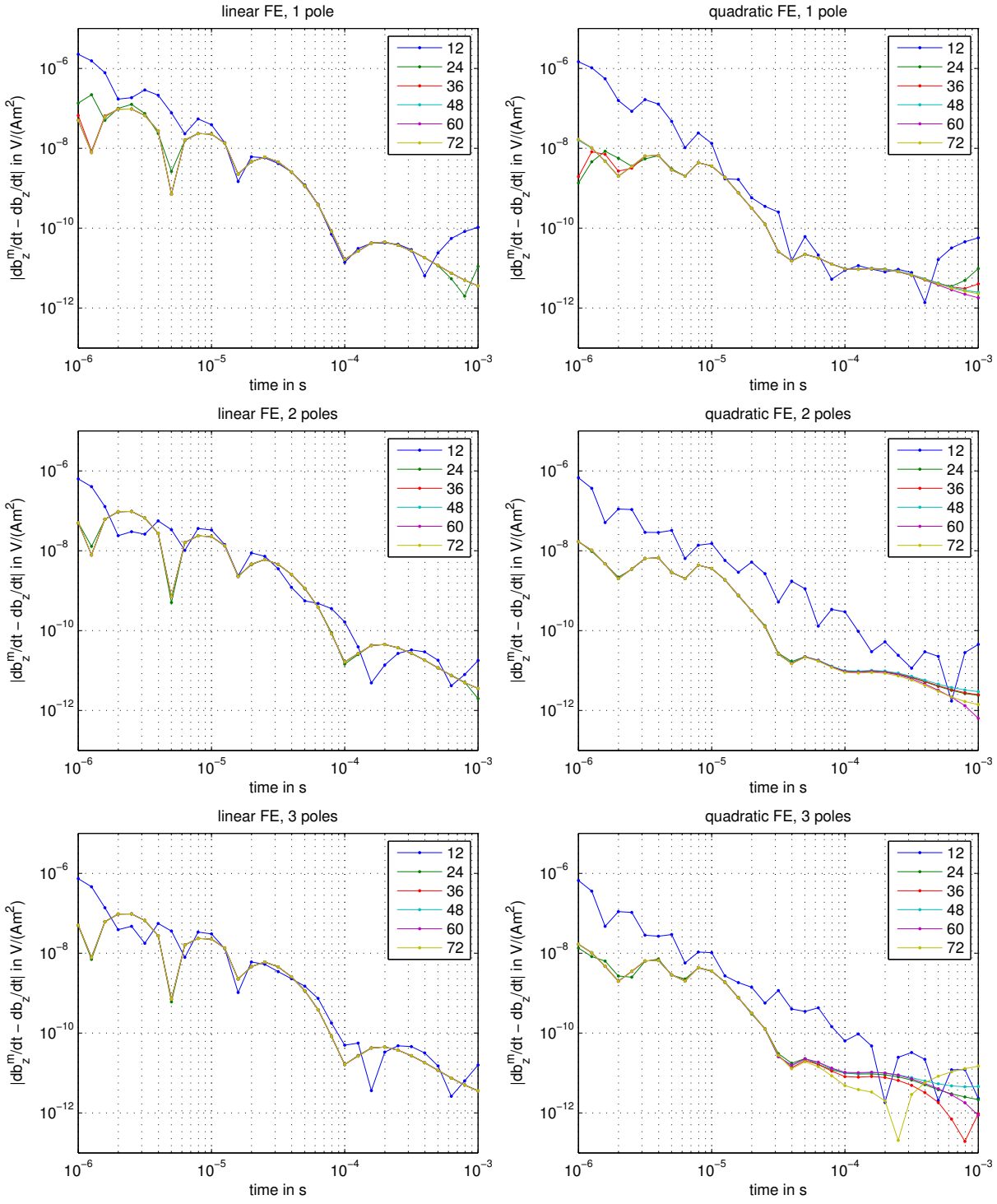

Figure 5. Absolute error between the transient $\partial_t B_z$ evaluated at $\boldsymbol{x} = (100, 0, 0)$ m extracted from rational Arnoldi approximations with $m - 1 = 12, 24, \ldots, 72$ and the transient obtained by the analytical solution for the layered half-space.

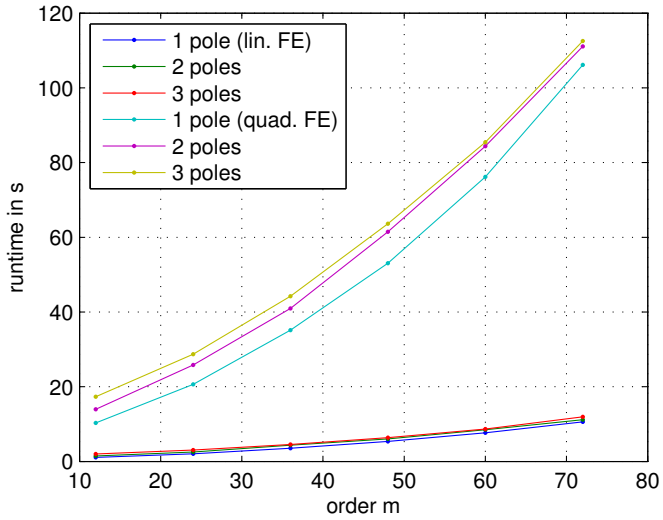

Figure 6. Plot of run times in seconds required to obtain a rational Arnoldi approximation of order m for linear and quadratic Nédélec elements and one, two and three cyclically repeated poles.

(a)

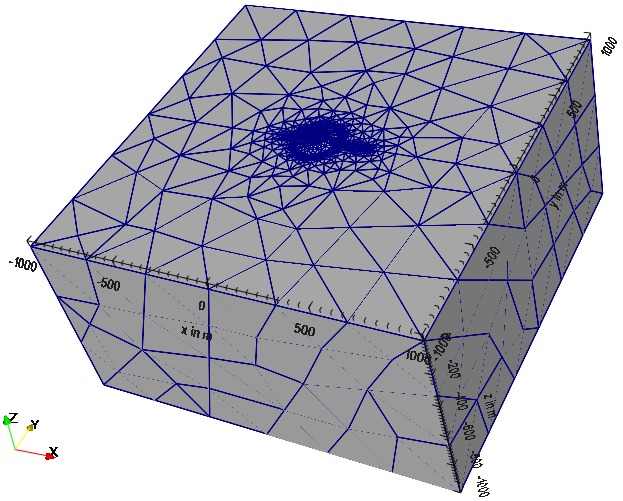

(b)

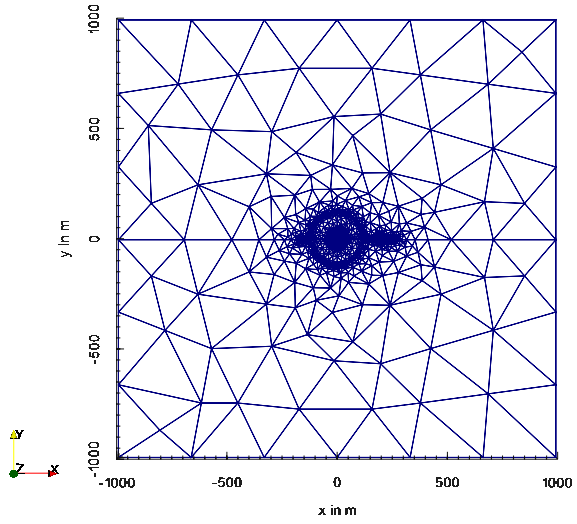

(c)

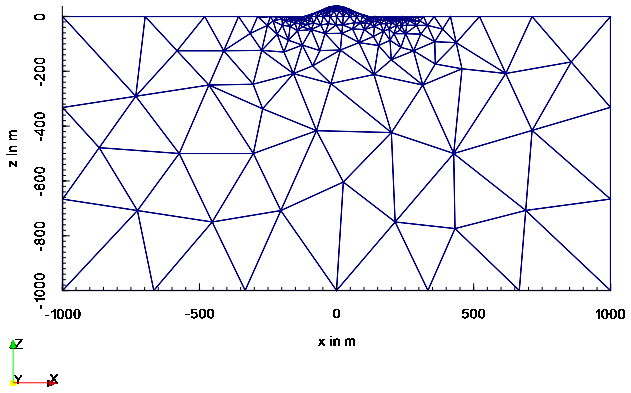

Figure 7. Trace of the tetrahedral finite element mesh used for computation of the transients: Perspective view (a), view from above onto Earth's surface (b), vertical slice along the plane $y = 0$ (c). The air layer, which has a thickness of 1000 m, has been omitted in all pictures.

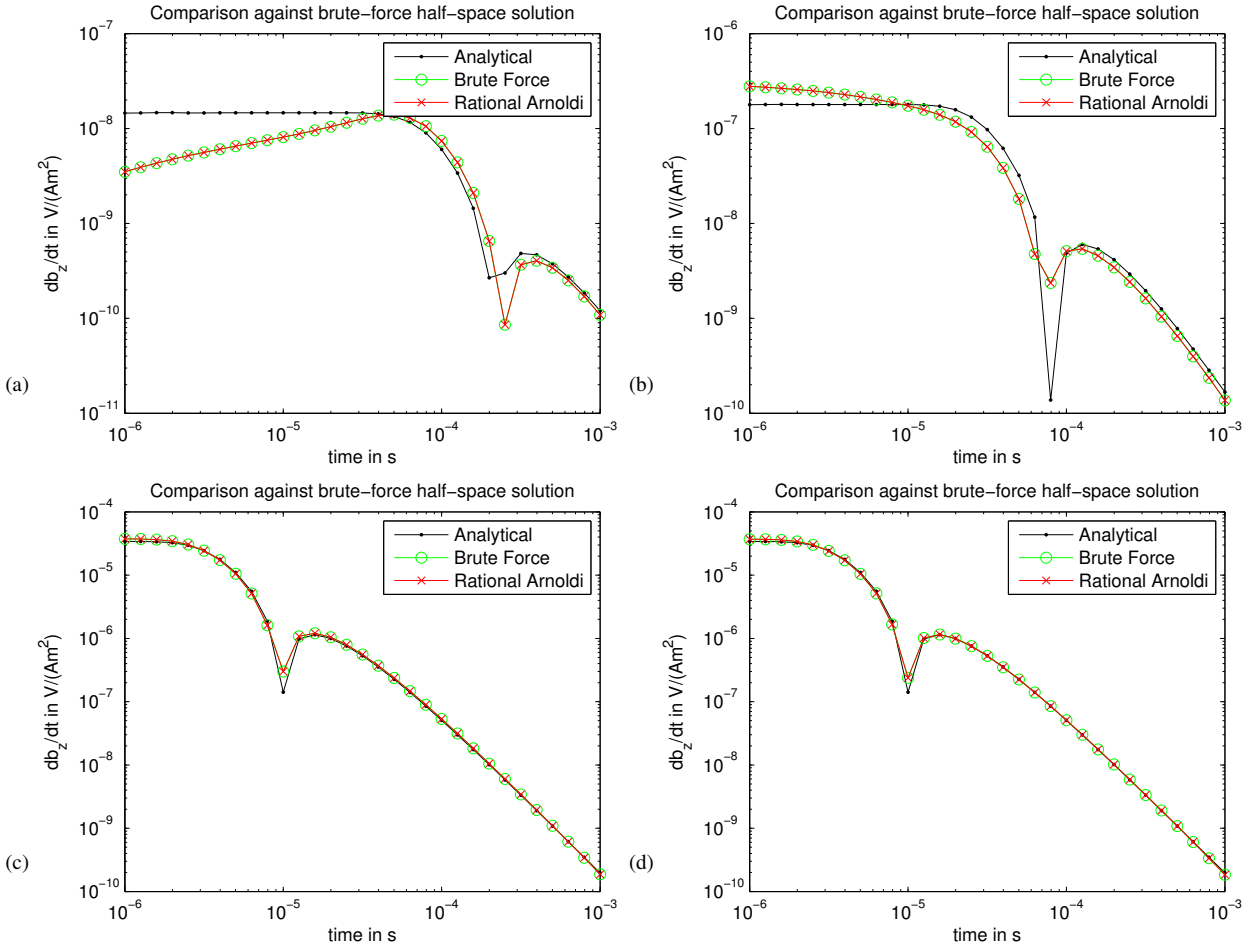

Figure 8. Comparison of transients $\partial_t B_z$ computed from a rational Arnoldi approximation of order $m = 36$ with an analytical solution, and a brute force solution obtained by inverse Fourier transform of frequency-domain solutions for the topography model, Nédélec elements of order $k = 2$, taken at the plane $y = 0$ at points $x = [-130, 0, 130, 270]$ m, and $z = [0, 38, 0, 0]$ m. The $20{\times}20$ m^2 transmitter loop source is centered at $x = 200$ m.

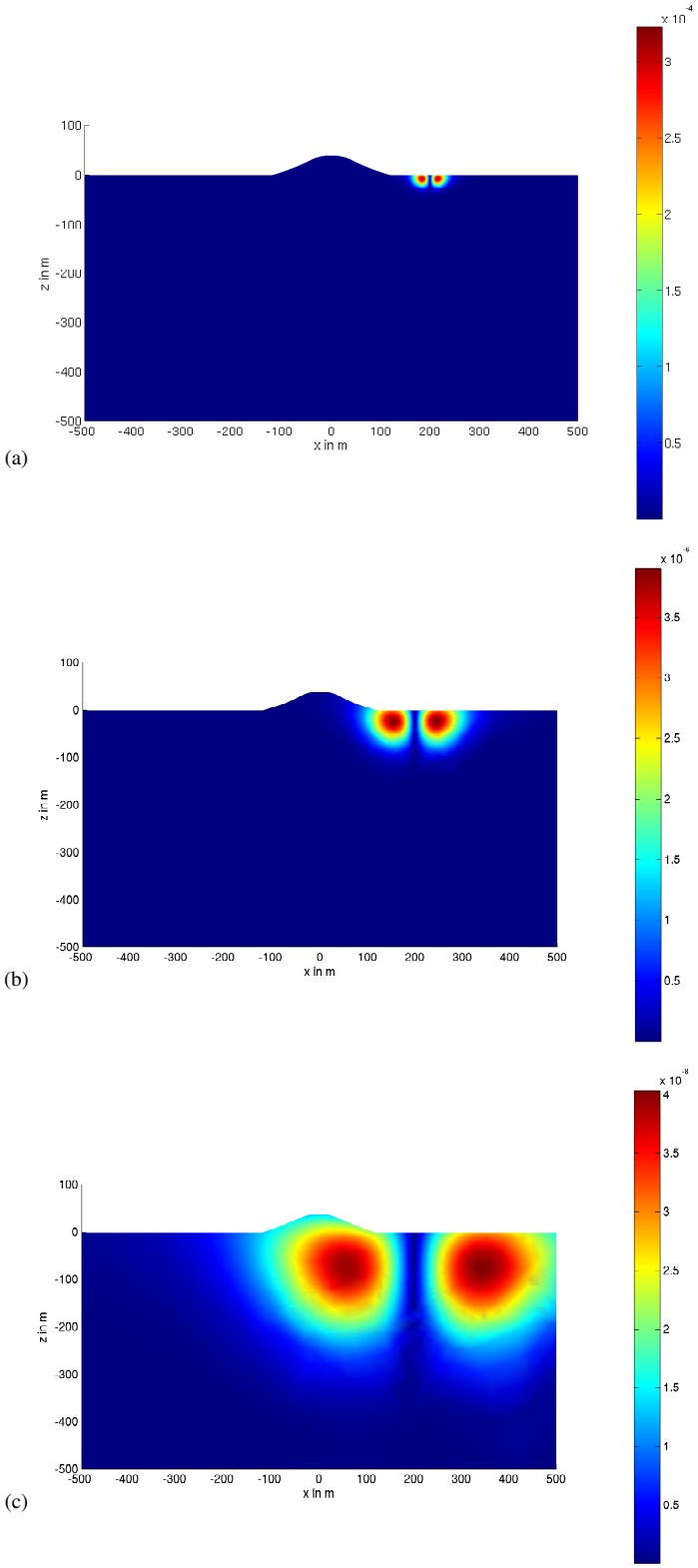

Figure 9. Snapshots of the induced current system given in A/m^2 at times $t = [10^{-6}, 10^{-5}, 10^{-4}]$ s taken at the plane $y = 0$ m.

LIST OF TABLES

Table 1. Table of parameters for building a rational Krylov space for approximating $f^t(z) = \exp(-tz)$ for all $t \in [10^{-6}, 10^{-3}]$ and $z \in [0, \infty]$. The column on the left corresponds to the dimension of the rational Krylov space minus 1. Each cell gives (an approximation for) the achievable uniform approximation error of $f^t(z)$ for all t and z, with the required cyclically repeated poles shown in brackets.

$m-1$	error (1 repeated pole)	error (2 repeated poles)	error (3 repeated poles)
12	1.71e-02 (-5.66e+04)	2.39e-03 (-1.26e+04, -7.88e+05)	2.39e-03 (-8.17e+03, -1.70e+05, -9.99e+05)
24	9.64e-04 (-1.13e+05)	1.33e-05 (-2.52e+04, -2.56e+06)	1.42e-05 (-8.36e+03, -2.41e+05, -5.23e+06)
36	2.94e-05 (-1.57e+05)	7.45e-08 (-3.32e+04, -3.88e+06)	1.05e-07 (-1.27e+04, -3.76e+05, -6.95e+06)
48	2.00e-06 (-2.14e+05)	4.87e-10 (-4.59e+04, -5.00e+06)	8.86e-10 (-2.06e+04, -4.23e+05, -1.23e+07)
60	1.02e-07 (-2.69e+05)	2.63e-12 (-5.40e+04, -6.30e+06)	6.88e-12 (-2.60e+04, -5.34e+05, -1.38e+07)
72	3.82e-09 (-3.14e+05)	2.11e-14 (-6.35e+04, -7.58e+06)	5.66e-14 (-2.60e+04, -6.73e+05, -1.96e+07)

$m-1$	error (4 repeated poles)
12	2.29e-03 (-7.04e+03, -3.35e+04, -7.61e+05, -7.61e+05)
24	1.21e-05 (-1.04e+04, -4.08e+04, -1.37e+06, -5.36e+06)
36	6.74e-08 (-2.76e+04, -4.08e+04, -2.45e+06, -6.51e+06)
48	5.08e-10 (-2.76e+04, -6.02e+04, -2.98e+06, -9.62e+06)
60	2.85e-12 (-4.08e+04, -7.32e+04, -4.41e+06, -9.62e+06)
72	2.23e-14 (-3.35e+04, -1.08e+05, -5.36e+06, -1.17e+07)

Table 2. Summary of runtimes for the layered half-space model, which consists of 24,582 tetrahedra.

Nédélec order	$k = 1$	$k = 2$
Problem size	$N = 27,623$	$N = 152,078$
Brute-force solution	66.36 s	739.14 s
Construction of decomposition (20) for three poles repeated 12 times	3.9 s	38.62 s
Evaluation of formula (21)	0.05 s	0.08 s

Table 3. Summary of runtimes for the topography model, which consists of 28,849 tetrahedra.

Nédélec order	$k = 2$
Problem size	$N = 181,302$
Brute-force solution	899.4 s
Construction of decomposition (20) for three poles repeated 12 times	44.86 s
Evaluation of formula (21)	0.09 s